Makhlouf *et al. Int J Concr Struct Mater* (2024) 18:45
https://doi.org/10.1186/s40069-024-00683-y

International Journal of Concrete Structures and Materials

RESEARCH

Open Access

Flexural Improvement of RC Slabs by FRP or Steel Using Different Strengthening Systems and Novel Anchoring Techniques

Mohamed H. Makhlouf[1*], Ibrahim A. El-Azab[1] and M. H. Mansour[1]

Abstract

An experimental study on reinforced concrete one-way slabs strengthened by various methods and materials is introduced in this paper. Innovative anchorage procedures are presented and evaluated to prevent the strengthening elements with FRP system from de-bonding at the initial stages. Externally bonded embedded in concrete cover (EBECC) strengthening technology was proposed to save the fiber strips from being subjected to heat, degradation, and sabotage. Nine RC one-way slabs, including a control slab and eight strengthened slabs, were cast. One RC slab was strengthened using externally bonded embedded in concrete cover (EBECC), whereas the other tested RC slabs were strengthened using either externally bonded (EB) or near-surface mounted (NSM) procedures. The following test variables are used in this study: the proposed anchors, the area of steel, the kind of material utilized in NSM rods (carbon fiber reinforced polymer (CFRP), glass fiber reinforced polymer (GFRP), and steel), and the strengthening scheme. The ultimate and initial cracking loads, load–deformation response, cracking patterns, and failure behavior were recorded and discussed. Additionally, a comparison of the stiffness, ductility, and energy absorption of the examined slabs was reported. The strengthened slabs by various techniques showed a boost in flexural strength that varied from 67 to 107% compared to the control slab. In addition, RC slabs strengthened by NSM-CFRP bars showed a maximum flexural capacity when compared with slabs strengthened by GFRP and steel bars. Also, the results supported the superiority of a novel end anchorage. The ABAQUS program was employed to conduct a finite element analysis (FEA) employing 3-D geometries to compare and assess the numerical performance of the identical slabs under similar test settings. The results showed good agreement between the experimental and numerical findings.

Keywords Near-surface mounted (NSM), Flexure, Externally bonded embedded in concrete cover (EBECC), Externally bonded (EB), Innovative anchorage

1 Introduction

Reinforced concrete (RC) structures may experience mechanical and environmental impacts, and excessive loading during the duration of their life due to changing design specifications and alterations in the buildings' intended uses. This is especially true for outdated structures. In addition, reinforcement steel rusting is one of the major widespread issues in existing buildings, and it has been discovered in numerous cases that slabs deteriorate to a level where they are weak in their ability to resist flexure. Therefore, they are unable to bear operational stresses for the entirety of their designated lifespan as this happens. Mostly, environmental and service variables are responsible for this, as they have the most influence (Zhou et al., 2021a). This may cause a crack or a reduction in the performance of these elements; therefore, strengthening and/or repair is required to increase

Journal information: ISSN 1976-0485 / eISSN 2234-1315.

*Correspondence:
Mohamed H. Makhlouf
mohamed.makhlouf@bhit.bu.edu.eg
[1] Department of Civil Engineering, Benha Faculty of Engineering, Benha University, Benha, Egypt

their capacity and performance. The difficulty is in performing efficient strengthening methods while taking several factors into account, such as the material, the degree of damage, the cost, the time, and so on (Thanoon et al., 2005). Strategies utilized for strengthening and repairing include the use of steel plates, RC jackets, aluminum strips, engineered cementitious composite, wire mesh incorporated into ferro-cement layers, and fiber reinforced polymer (FRP) in many forms such as sheets or plates or bars. Numerous approaches and materials have been investigated in recent decades to enhance reinforced concrete construction elements (Ali & Yehia, 2016; Choi et al., 2022; Correia et al., 2017; El-Mandouh et al., 2023; Fernandes et al., 2017; Hu et al., 2019; Khalil et al., 2022a; Makhlouf et al., 2023; Ngidi & Dundu, 2018; Shaheen & Abusafa, 2017; Tank & Modhera, 2017).

Fiber reinforced polymer (FRP) materials offer various features: a substantial strength-to-own weight ratio, for instance, efficiency for rusting opposition, and easy installation for usage. FRP materials have gained popularity in recent years for their use in strengthening different structural elements. They have been widely applied by using several effective strengthening strategies to fortify various RC elements that are susceptible to straining action such as bending moment, normal stresses, shear, torsion, earthquake, and so on (El-Mandouh et al., 2022; Laraba et al., 2014; Rageh et al., 2022; Wang & Tan, 2002; Yehia et al., 2023; Zhou et al., 2020). The two foremost FRP methods of application are: (i) the externally bonded (EBR) scheme, where the strengthening item is attached over the prepared outer face of the concrete (Anil et al., 2013; Zhou et al., 2021b), and (ii) the near-surface mounted scheme, which the fiber element is anchored in grooves created in the concrete cover (El-Gamal et al., 2016; Galati & Lorenzis, 2009; Lorenzis & Teng, 2007; Sharaky et al., 2014). Those systems have become popular for increasing the capacities and improving the behavior of reinforced concrete elements. The adhesive material is used to attach the FRP (sheets/strips/bars) to the flexural side of the RC element, thereby reinforcing and strengthening the elements that experience flexural forces.

Nevertheless, a crucial point that frequently lowers the objective capabilities for the strengthening process is the separation of the fiber from the RC element. Whenever applying the NSM methodology, fiber elements are embedded in slots that were previously carved inside the concrete cover, and then the empty spot within, which is between the FRP and the concrete holes is stuffed with epoxy resin adhesive, allowing more effective action outcomes when compared to the EB techniques (Makhlouf & Mansour, 2023). Further, the NSM system has several possible advantages, including enhanced FRP defense from external influences, suitability for strengthening the area affected by negative bending moments, and a reduction in changes to the building's visual appeal. The structural performance of RC elements fortified by the NSM strategy has been tested in recent research under a variety of study variables, which include bond performance (length, grooves size, adhesive kind), shapes, materials, the strength of concrete, and loading installation. Numerous test results revealed that employing the NSM method for strengthening the elements led to considerably enhanced performance and flexure capacities (Amin & Khan, 2022; Barris et al., 2020; El-Gamal et al., 2016; Failed, 2020; Khalil et al., 2022b; Makhlouf & Mansour, 2023; Sharaky et al., 2014).

Generally, the NSM is a successful method for strengthening the RC slabs. The effectiveness of the ligament ability between the strengthening bars and the existing RC elements determines the flexure capacities. The glue used, the length of the connection, the size and type of filler used in the grooves, the surface roughness, the bar size and shape, and the surface layout of the bars all affect the bond's quality (Amin & Khan, 2022; Failed, 2020; Makhlouf & Mansour, 2023; Muciaccia et al., 2022; Smith et al., 2011; Yang et al., 2018). Since end anchors were not used in a lot of research investigations that strengthened RC slabs using NSM techniques, it was noted that the capacity of strengthened slabs was constrained by fast bond breakdown.

The application of the EB FRP system to increase the flexural strength of RC one-way slabs was studied experimentally and numerically by Elsanadedy et al. (Elsanadedy et al., 2015). Eight slabs were tested to explore the impact of using adhesively bonded pultruded, precured CFRP plates and unidirectional carbon fiber fabric impregnated with an epoxy resin for enhancing flexural strength. According to the experimental and numerical outcomes, RC one-way slabs' ductility is reduced while their flexural capacities and stiffness are increased by the EB FRP system, the increase in the width of FRP laminate is more effective than the thick. Moreover, Shehab et al. (Failed, 2017) studied the impact of using FRP sheets for upgrading the flexural strength of one-way slabs with openings. The experimental program consisted of five slabs with different lengths of CFRP strips. The predominant form of failure was CFRP strip de-bonding, with stress being applied to the steel bars adjacent to the cutout. Debonding of the FRP sheets is the major issue concerning using FRP sheets for flexural strengthening and the full strength of FRP sheets has not been exploited.

Strengthening using a hybrid combination of carbon fiber laminates and steel plates in different ways was studied by Zheng et al. (Zheng et al., 2019) to mitigate the de-bonding issue of adhering to FRP sheets. Nineteen specimens were tested with different strengthening schemes. Test results revealed that the hybrid strengthening strategy utilizing CFRP and steel plates with overlaps layout had the highest rigidity and capacity when compared to independently reinforced designs. Moreover, none of the laminates had any contact detachment. Afefy et al. (Afefy & Fawzy, 2013) conducted an experimental study to determine the effects of adding an opening around the center patched load in a one-way slab strengthened with CFRP, NSM bars, and ECC overlay in different arrangements. Every strengthened slab exhibits a higher flexural strength compared to the control slab. Among the strengthening techniques, the RC slab reinforced with CFRP demonstrates the highest flexural capacity.

The performance of RC one-way slabs strengthened by EB and NSM techniques using FRP, or steel materials has been studied in some research works but was limited. Although there are only a few researches available, using an end anchoring system might prevent early de-bonding or lead to being late. Furthermore, in the externally bonded system, FRP (sheets/strips) are exposed and susceptible to sabotage, destruction, variations in temperature, and other factors. So, the behavior of the FRP might change. In this study, FRP strips were protected in the wide groove which was created by removing a part of the concrete cover of the slab, then fastened in place before the cuts were filled with grout, as a specialized cement mortar. This new strategy is called the externally bonded embedded in concrete cover (EBECC) strengthening technique. In addition, an innovative NSM steel bar end anchorage system is presented. Also, the GFRP spike anchors for the EB-FRP sheets were employed.

Based on the aforementioned literature, there is a lack of information on the flexural response of RC one-way slabs strengthening with novel strengthening techniques that could mitigate the traditional methods. The main intent of this research is to: evaluate the impact of using different materials with innovative anchorage techniques for strengthening RC slabs under bending; and validate the design equations related to nominal flexural capacity in current codes and guidelines.

2 Study's Purpose

The substantial aim of this study is to assess the influence of novel strengthening methods on the flexural strength of reinforced concrete slabs strengthened with various techniques and materials. The impact of the subsequent factors is examined in this research: (a) the strengthening strategies (EB, NSM, and EBECC); (b) the material of NSM rods used (glass, carbon, steel); (c) the area NSM-steel used; (d) the proposed end anchors (had or hadn't end-anchor); and (e) the anchoring system (without anchor or with anchor, where the strands with collections of glass fiber shaping a blade over the strips as the anchors). ACI 440-2R-17 was used to forecast the flexural capabilities of the experimentally tested slabs (ACI, 2017). Additionally, NLFE simulations were applied to verify the software-assisted response of the tested specimens by utilizing the ABAQUS program (Bassam Qasim Abdulrahman, 2021).

3 Experimental Investigation

3.1 Slabs Details

Three groups of nine RC slabs were included in the experimental investigation. One control slab (Group No. 1), and eight slabs strengthened by different methods in Groups No. 2 and 3. The inner reinforcing steel and the concrete dimensions were identical for all slabs. The effective span was 1400 mm, all specimens were 600 mm wide, 100 mm in depth, and had an overall length of 1600 mm. High tensile steel reinforcement of 10 mm diameter was employed for the flexural reinforcement 6 bars in the main long direction and 8 bars in the secondary reinforcement as presented in Fig. 1.

3.2 Slabs Scheme Description

The objective of this study was to investigate the performance of reinforced concrete (RC) slabs strengthened on the tension side using different techniques. A total of nine RC slabs were constructed and examined as the experimental program, divided into three groups. Group one consisted of a control slab (S-C) with no strengthening, serving as a reference specimen. Group two included three slabs strengthened with three strips of glass fiber reinforced polymer (GFRP). One slab was strengthened using the externally bonded (EB) technique without anchors (S-G-3ST), another slab was strengthened using the EB technique with anchors (S-G-3STA), and the third slab in this group was strengthened using the innovative externally bonded embedded in concrete cover (EBECC) approach (S-G-3STM). In Group 3, five slabs were examined. Three slabs were strengthened with three 10 mm bars: one with glass fiber reinforced polymer (GFRP) (S-G-3G10), one with carbon fiber reinforced polymer (CFRP) (S-C-3C10), and one with steel (S-S-3R10). Another slab in this group was strengthened using three near-surface mounted (NSM) 12 mm steel bars (S-S-3R12). The remaining slab in Group 3 was strengthened

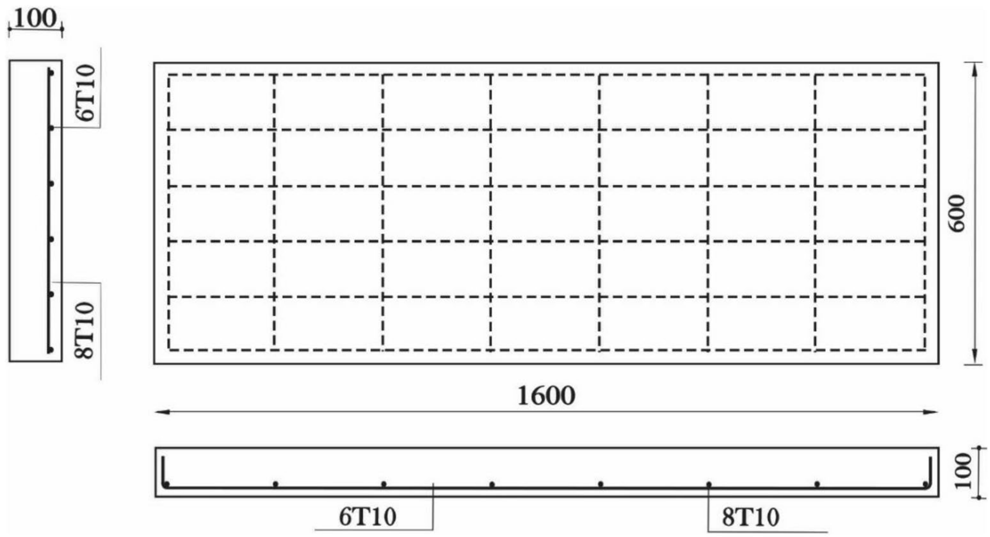

Fig. 1 Internal reinforcement details and concrete dimensions of tested slabs

with three 10 mm steel bars (S-S-3R10III) and featured a novel end anchoring system introduced in this research.

All the slabs were intentionally designed with under-reinforcement criteria to ensure flexural collapse during testing. The specifications and characteristics of the specimens are provided in Table 1.

3.3 Materials Properties

3.3.1 Concrete

Standard cubes with sides measuring of 150 mm used concrete have been cast with each slab and left to cure until the testing day to determine its strength. Consequently, the concrete utilized in this investigation had an average compressive strength of 30 MPa. Naturally local sand having a specific weight of 2.60, ordinary Portland cement (42.5 class), and crushed dolomite having an average size of particles of fourteen millimeters, and freshwater were the ingredients for producing the concrete mixture. Table 2 lists the components used to prepare one cubic meter of concrete and the average compressive and splitting tensile strength.

3.3.2 Steel bars

The elasticity modulus (E) of the high tensile deformed steel rods, which were employed for both the internal reinforcement and external strengthening NSM bars, was equivalent to 200GPa, the characteristics of the steel reinforcement utilized in this paper are presented in Table 3.

3.3.3 GFRP Strips

Sika Company's unidirectional knitted glass fiber composite GFRP was used as an externally bonded strengthening element. An epoxy glue with a uniform layer of

Table 1 Slabs matrix

Group	Slab code	System	Material	`Scheme
1	S-C	–	–	Un-strengthened slab—Control
2	S-G-3ST	EB	GFRP	Slab strengthened by 3-strips without anchors
	S-G-3STA	EB	GFRP	Slab strengthened by 3-strips with anchors
	S-G-3STM	EBECC	GFRP	The slab was strengthened by three strips inside the notch and then wrapped by mortar cover
	S-G-3G10	NSM	GFRP	Slab strengthened by three 10 mm NSM GFRP bars
3	S-C-3C10	NSM	CFRP	Slab strengthened by three 10 mm NSM CFRP bars
	S-S-3R10	NSM	Steel	Slab strengthened by three 10 mm NSM steel bars
	S-S-3R12	NSM	Steel	Slab strengthened by three 12 mm NSM steel bars
	S–S-3R10III	NSM	Steel	Slab strengthened by three 10 mm NSM-steel bars with end anchorage (III—shape)

Table 2 Components of one cubic meter of concrete mixture

Ingredient	Cement (kg/m^3)	Fine aggregate (kg/m^3)	Coarse aggregate (kg/m^3)	Water (kg/m^3)	Average compressive strength (MPa)	Average splitting tensile strength (MPa)
Mix	350	650	1360	170	30.2	3.74

Table 3 Characteristic of steel reinforcement

Diameter (mm)	Cross section area (mm^2)	Yield strength (MPa)	Ultimate strength (MPa)
10	78.5	570	785
12	113.04	410	680

thickness of 2 mm was used to attach the GFRP strips to the RC slab. It is necessary to remove any loose material from the concrete surface before weaving the GFRP component into the RC slabs. A special roller was used to press out any extra adhesive and air bubbles when installing the fiber weave on the concrete surface and keep the epoxy layer thickness uniform throughout the whole span. The characteristics of the GFRP strips that were used are shown in Table 4. The Sikadur-330 adhesive, which is a mixture made up of two epoxy compounds, was used. To verify their consistency before use, they are mixed and swiftly blended. The mechanical characteristics of the applied adhesive are listed in Table 5.

3.3.4 Fiber Rods

The general properties of the GFRP and CFRP rods utilized in this investigation are shown in Table 4. The slabs were strengthened using ten-millimeter nominal diameter GFRP and CFRP as near-surface mounted fortifying. The manufacturer used the pultrusion technique for producing the FRP bars, subsequently followed via a coating procedure applied to the FRP bars' surface.

3.3.5 Sika-Grout 214 Mortar

A unique cementitious-based mortar called Sika-grout 214 was used to fill in the grooves in the concrete slab, strengthened using the EBECC method. The goal is to shield the EBECC system's strengthening layer from exposure to acts of vandalism deterioration, heat, environmental influences, etc. Additionally, the surface of the slab did not clear after the strengthening system was produced. High compressive strength, flexibility, non-shrinkage, and self-compaction are a few benefits of the concrete mortar. The strength of the mortar is displayed in Table 6.

Table 5 Adhesive's characteristic and properties (Sikadur-330)

Property	Amount
Compressive strength (MPa)	110
Resins strength on reinforcement (MPa)	26
Resins strength on RC (MPa)	2 (concrete failure)
Modulus of elasticity (MPa)	12,800

Table 4 FRP composites' characteristics

4-i) Fiber rods		
Characteristic	**Carbon-FRP-rods**	**Glass-FRP-bars**
Size mm	10	10
Nominal area mm^2	78.5	78.5
Tensile stress MPa	1560	1165
Elasticity modulus (E) MPa	215000	65000
Elongation at rupture	1.25	2.20
4-ii) Glass fiber woven (uni-directional)		
Property		**G-FRP**
Thick. (mm)		0.170
GFRP strips wide (mm)		100
Tensile strength MPa		2250
Elasticity modulus (E) MPa		76,000
Elongation at rupture		2.80%

3.4 Implementing Strengthening Schemes

This section describes the application procedures for the different strengthening techniques employed in the second and third groups. The steps involved in each method are outlined below.

It is worth highlighting that GFRP strips used in the second group were 0.17 mm thick, 100 mm broad, and 1000 mm long.

3.4.1 Slabs Strengthened by EB-GFRP (Without/With) Anchors

The following procedure was utilized to attach the EB-GFRP strips to the specimen (S-G-3ST): (1) grinding the surface of the strengthening slab's bottom face until the coarse aggregates is exposed. (2) Washing and using air-brushes on the concrete surface to remove concrete dust and other debris. (3) Following purging, a regular layer of the adhesive was put on the slab's side, followed by the placement of the GFRP sheet on the RC slab and evenly tightly compressed to establish a flawless connection with the slab.

For the specimen (S-G-3ST) the previous steps from 1 to 3 were used to attach the GFRP strips on the slab (S-G-3STA), in addition to 6 GFRP anchors with a 10 mm diameter. The employed GFRP anchors were subsequently installed in the following sequence: (4) using an electric drill to perforate the designated holes of 50 mm depth into the RC slab. (5) Employing an insufflator with an inclined slope that enables the full clearing of any particle scraps left into pre-drilled holes. (6) The glass fiber anchorages, were fabricated using a piece of the GFRP weave, cut rolled and placed into the already drilled pit, and the anchorages edges were then formed into a fan shape on top of the GFRP strips. (7) It should be noted that the strengthening strip used for anchoring were manufactured from the same GFRP. The applied anchorages were dipped into adhesive prior to set in holes, and the anchorages were 6 and spaced along the GFRP strips at 180 mm intervals (CL to CL). (8) The installation process guarantees that the anchoring and strengthening components work together as a single unit, therefore failure caused by the separation of the GFRP strips could be avoided or delayed.

Table 6 Cement mortar's mechanical characteristics

Tested age (days)	Compressive strength (MPa)	Flexural strength (MPa)
7	36	4
28	58	11.4

3.4.2 Slab Strengthened by EBECC—Technique

The last slab in the second group, (S-G-3STM) was strengthened using the innovative technique externally bonded embedded in concrete cover (EBECC), which involved: (1) using a grinding procedure to carve a groove in the slab's flexure face "tension face". (2) Using the same approach as the EB method mentioned above, three GFRP strips with a 100 mm width and 0.17 mm thickness were employed in the lengthwise direction at the flexure face had a 1000 mm long in the middle span. (3) The glass fiber strips were also textured by sand covering, and the contact zone of the concrete slab within the strips was roughened with a chisel to eliminate the cement cover and reveal the rough particles. (4) The joint portion of the slab was disinfected using air under considerable pressure and was then sufficiently moistened prior to the cementation mortar cover (Sika-grout 214) being applied. The groove was fully stuffed with Sika-grout 214 mortar then the outer face was smithed.

3.4.3 Slabs Strengthened with NSM technique

The specimens contained in group # 3 have been strengthened by utilizing the NSM technology. Firstly, using a saw blade machine, slots were first cut into the slabs' lower faces. Each slot had an exact depth and width of 15 mm, as well as an identical section and square form. After that, compressed air was blown into the drilled grooves to remove any fine dust. Then epoxy paste was added in the grooves, the grooves were filled nearly halfway, the NSM bar was inserted, and then gently pushed to let the glue flow around the bar and properly cover any gaps between it and the groove's edges. The groove was stuffed with more epoxies paste once placing the NSM bars, the entire surface was then leveled and smoothed. The strengthened specimens are followed by at least a 7-day cure before testing.

Fig. 2 depicts the elements used in the enhancing methods, Fig. 3 includes some images of strengthening techniques being applied before and after implementation. Fig. 4 depicts the specifics of the strengthening slabs.

3.5 Measurement and Testing Setups

The testing was done using the outfitted, three-dimensional steel frame shown in Fig. 5. The vertical deflection was monitored using a 100-mm LVDT. Three points—one in the middle of the span and one 200 mm to the left and one 200 mm to the right of the specimen's center line—were utilized to gauge the downward deflections.

Through the use of a load cell, the slabs were evaluated under two-line loads, the slab was repeatedly loaded until it failed. The slab was loaded using a 1000-kN capacity loading cell. The vertical deflections were measured

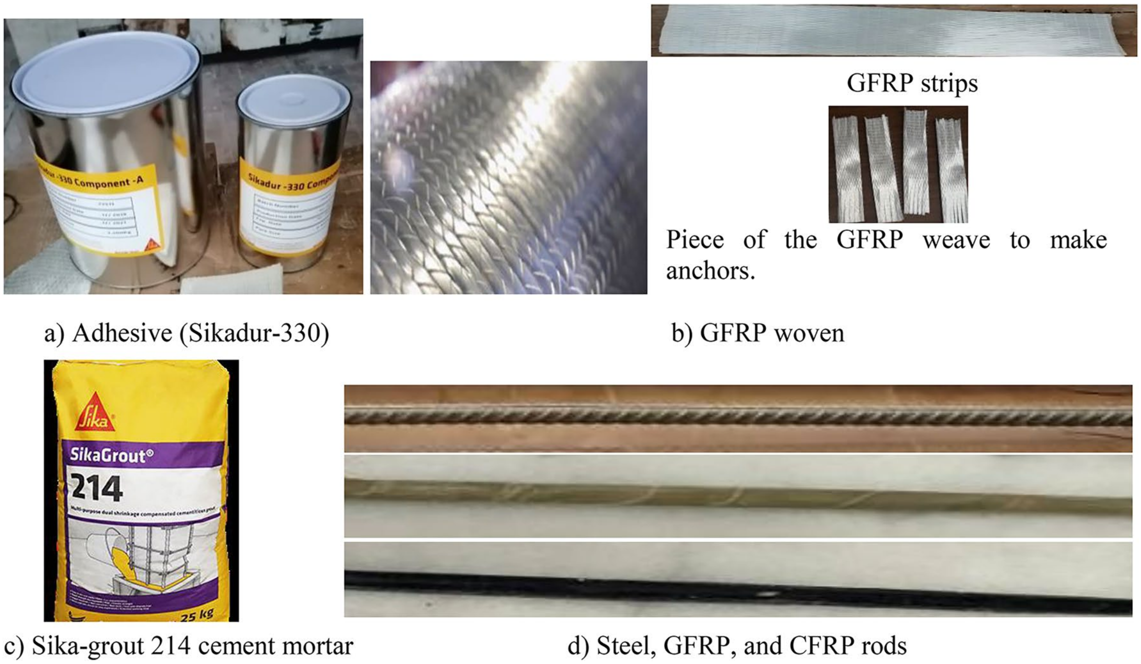

Fig. 2 Materials used for strengthening in this study

following each loading stage. All slabs were loaded at a rate of 0.5 to 0.7 kN/s. During the test, output from both LVDT and load cell systems were recorded and stored using an automated data logger device.

4 Experimental Findings and Discussion

To evaluate the efficiency of the adopted strengthening procedures and reveal the effects of the factors taken into consideration in this work, the behavior of the tested slabs both un-strengthened and strengthened were compared based on the outcomes of experiments. In general, the flexure performance of the enhanced slabs by various systems was higher than that of the control slab that was not fortified. The findings for the examined slabs are summarized in Table 7. A discussion of the findings is provided in the sections that follow.

4.1 Failure Modes and Cracking Behavior

To investigate the cracking and inadequate actions, the initial cracking was noted for each slab in this study, and the propagating of cracks observed was tracked, and the mode of failing is identified. In general, the first fracture was seen to form in the center, and as the increased, more cracks appeared. In the strengthened slabs, a greater number of cracks were seen before failure. Five distinct failure mechanisms have been discovered in this study caused by the experimentally noticed behavior, and they are as here: (a) normal-flexural mode (F-M); (b) flexural-debonding mode (F-D-M); (c) flexural-rupture mode (F-R-M); (d) flexural-shear mode (F-S-M); and (e) flexural-shear-debonding mode (F-S-D-M). Fig. 6 depicts the tested slabs' typical failure modes and Table 7 provides the mode of failure for each specimen.

4.1.1 Normal–Flexural Mode

The flexure reinforcement reached the yield limitation, causing the concrete to be crushed in the compression zone during the collapse. This occurred in reference slabs (S-C) and beams (S-G-3STM) strengthened using the EBECC technique. The reference slab failed near the center, while S-G-3STM had more distributed cracks with lower average widths. The flexural response increased at the greatest stress to break in the space between applied loads.

4.1.2 Flexural–Debonding Mode

The tested slab (S-G-3ST) matched the reference specimen's cracking pattern, with cracks appearing along the balancing axis and increasing load. The specimen's mode of failure involved partially de-bonding GFRP strips and steel yielding, primarily due to loss of joint action between the strips and the slab's face.

(a) Slabs strengthened by EB- technique (without/with) anchors

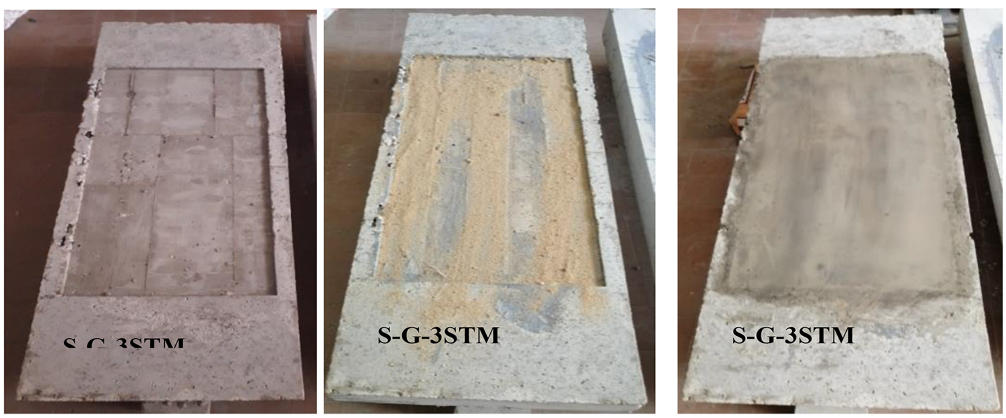

(b) Slab strengthened by EBECC - technique

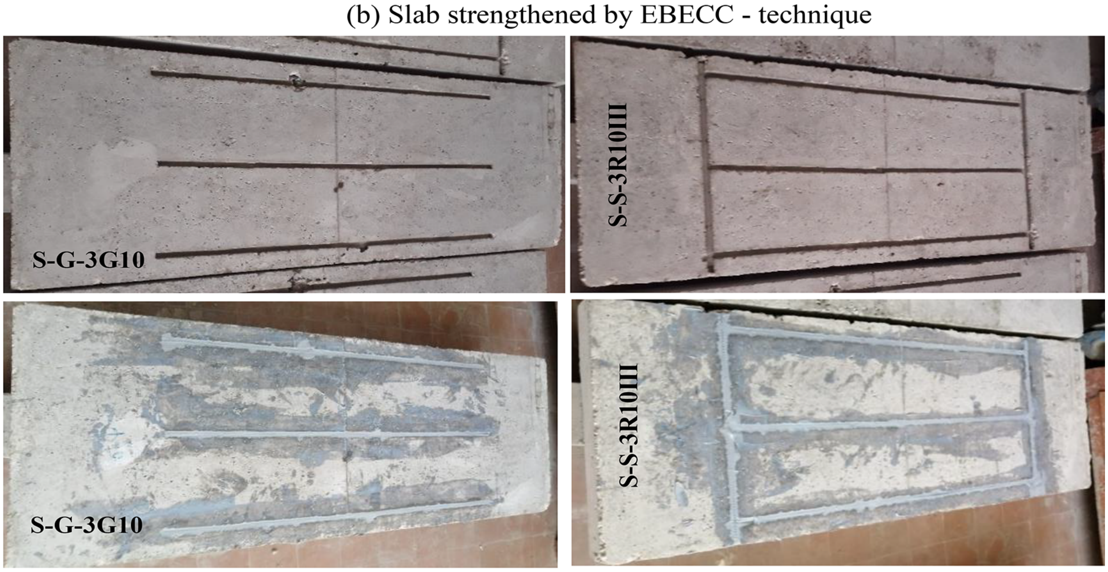

(c) Slabs strengthened by NSM- technique (without/with) end anchorage

Fig. 3 Preparing of various strengthening techniques

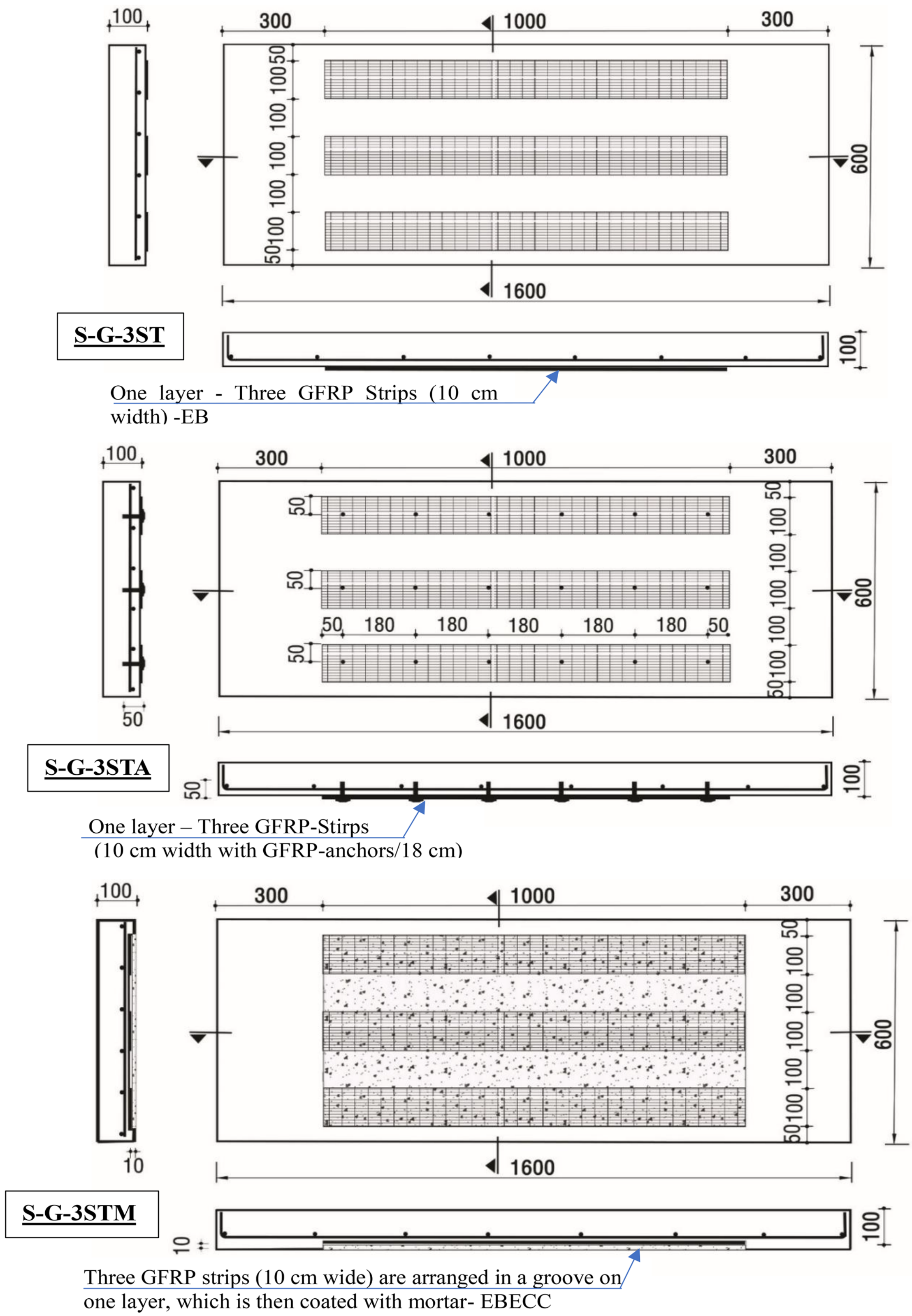

Fig. 4 Detailing of the proposed strengthening arrangement

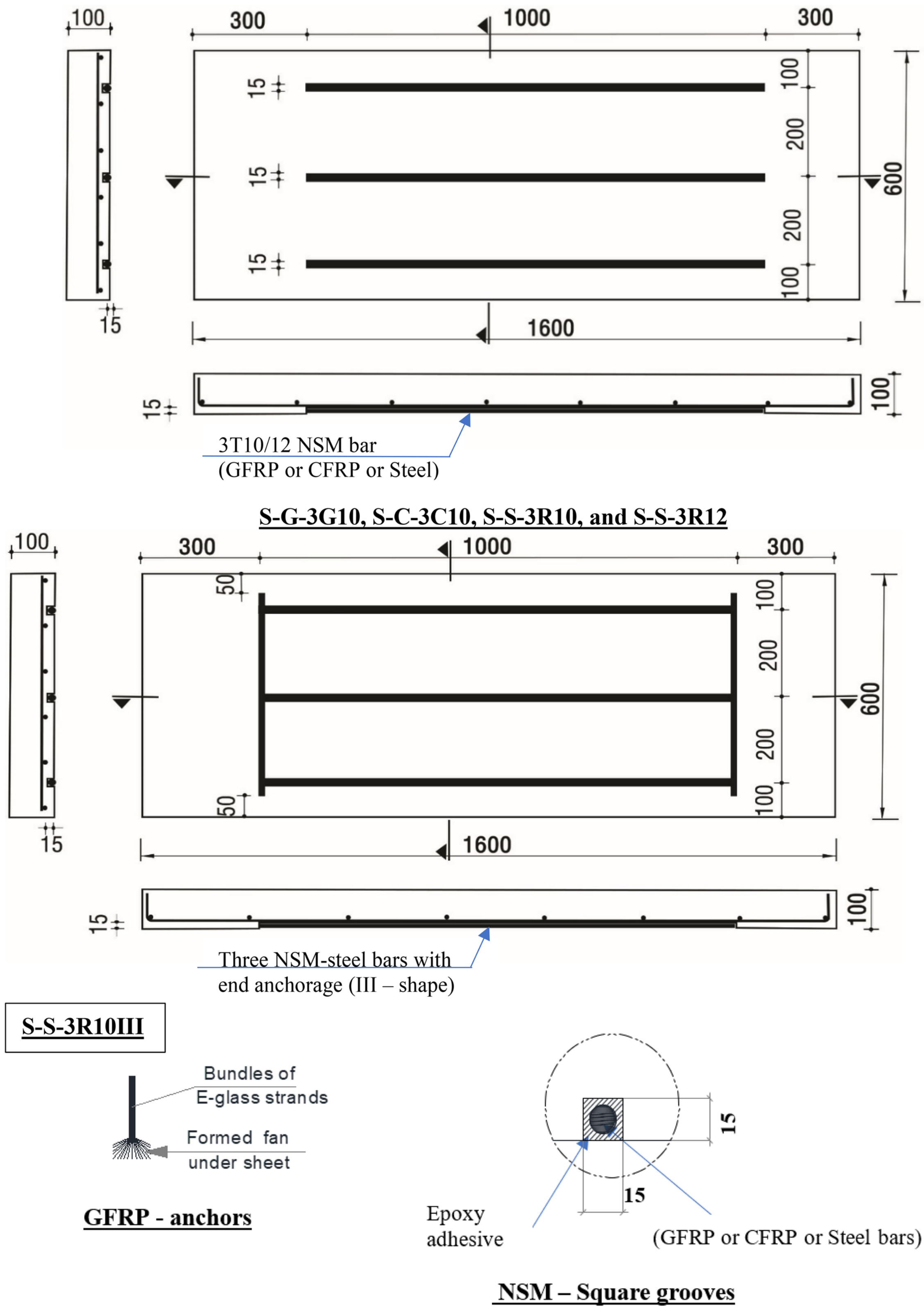

Fig. 4 continued

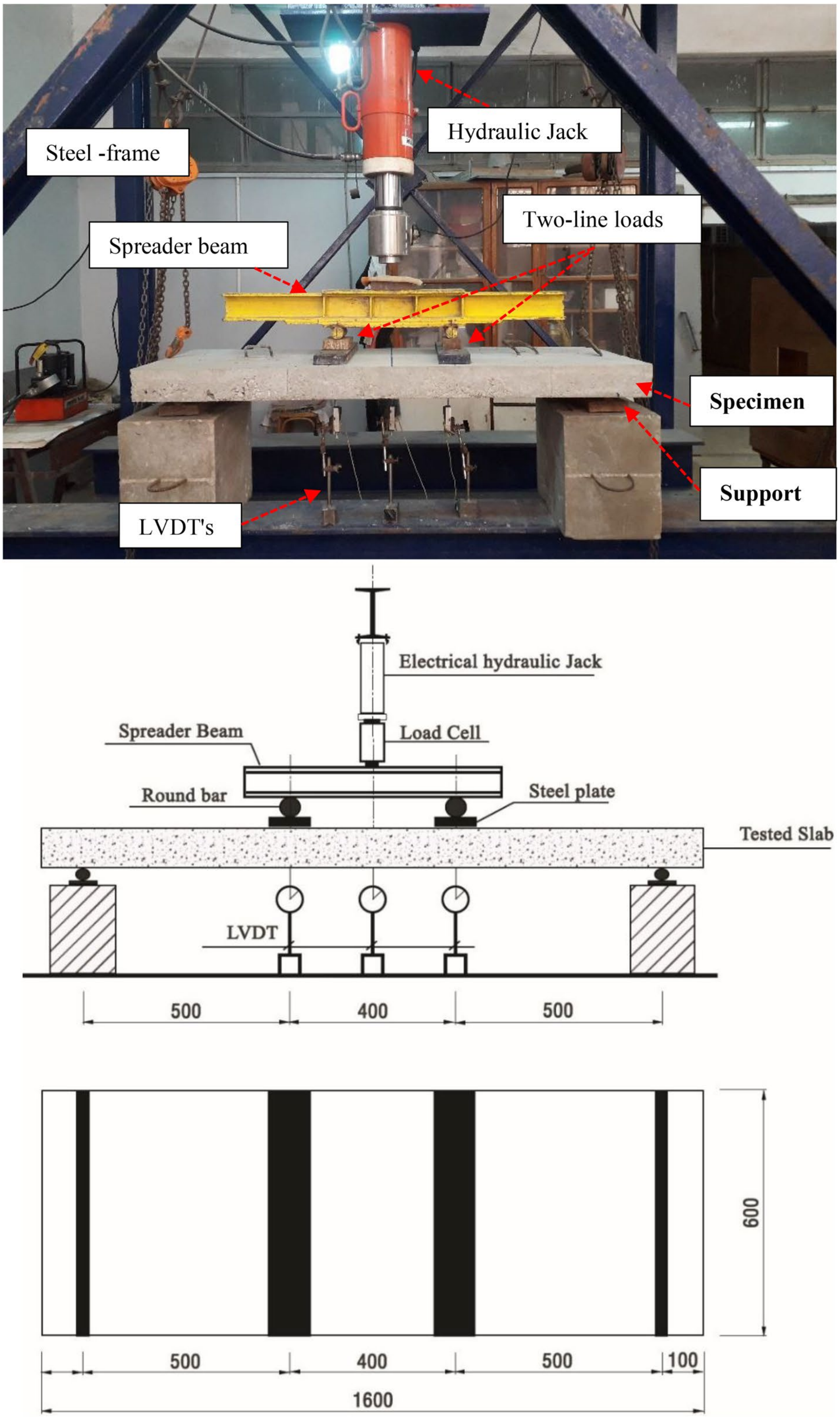

Fig. 5 Setting up experimental tests and placing LVDTs

Table 7 Experimental findings outline

Slabs	Cracking		Ultimate		Δ at 45 kN (mm)	(P_u/P_{uR} -1) (%)	Reduction of def. (%) $\Delta_{ul}/\Delta_{ul\ Ref.}$ at 45 kN	DI	Ki kN/mm	Ku kN/mm	E_{tot} kN.mm	Mode of failure
	P_{cr} kN	Δ_{cr} mm	P_u kN	Δ_u mm								
S-C	25	4	45	12	13.5	–	–	3.38	6.25	2.11	363	F-M
S-G-3ST	40	4	78	15.3	4.8	73.33	60.00	3.83	10	3.36	724	F-D-M
S-G-3STA	43	3.6	86	15.3	4.2	91.11	65.00	4.25	11.9	3.68	998	F-R-M
S-G-3STM	45	3.5	87	18.2	3.5	93.33	70.83	5.20	12.9	2.86	1278	F-M
S-G-3G10	45	4.1	81	14.5	4.1	80	65.83	3.54	11	3.46	572	F-S-D-M
S-C-3C10	50	3.9	87	14	3.1	93.33	74.17	3.59	12.8	3.66	581	F-S-D-M
S–S-3R10	41	3.7	75	16.1	4.25	66.67	64.58	4.35	11.1	2.74	626	F-S-D-M
S–S-3R12	45	3.6	82	16.5	3.8	82.22	68.33	4.58	12.5	2.87	927	F-S-D-M
S–S-3R10III	55	3.7	93	18	2.5	106.7	79.17	4.86	14.9	2.66	1031	F-S-M

$K_i = \frac{P_{cr}}{\Delta_{cr}}$, $K_u = \frac{P_{ul}-P_{cr}}{\Delta_{ul}-\Delta_{cr}}$, K_i is the uncracked stiffness, K_u is the ultimate stiffness, DI is the ductility index

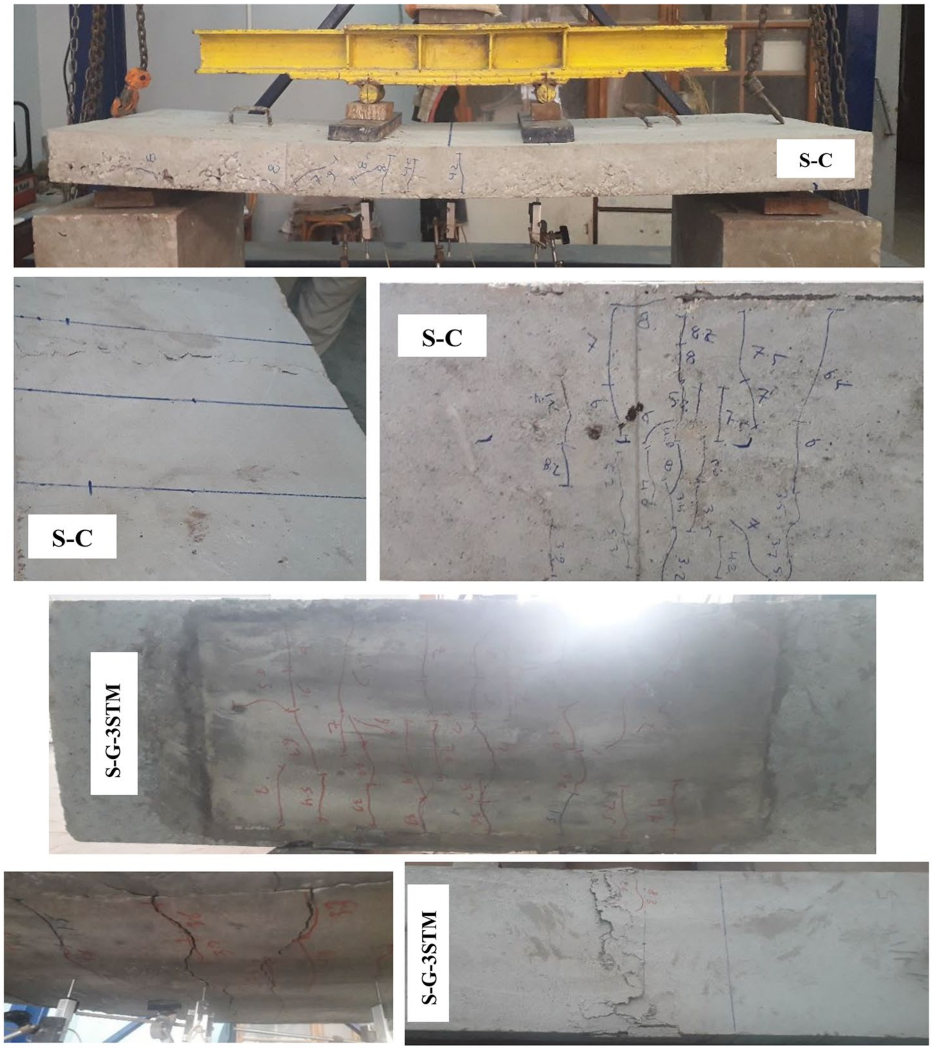

(a) Normal-flexural mode "yielding the main reinforcement, then concrete crushing in the top at failure."

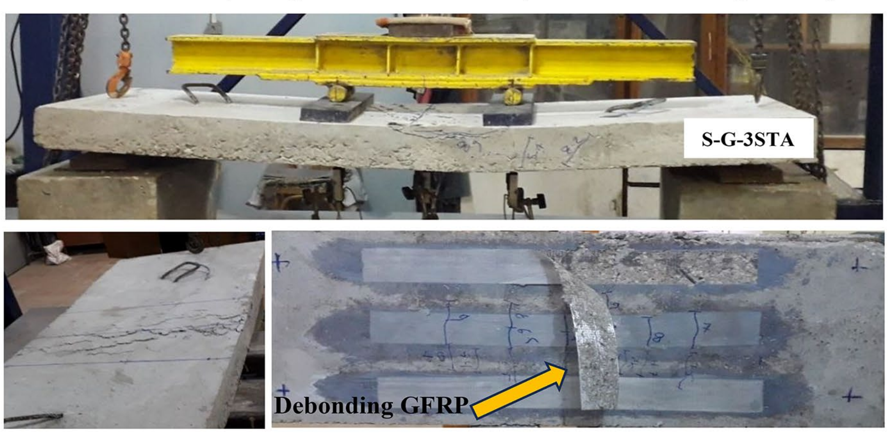

(b) Flexural - debonding failure " normal-flexural, then de-bonding of the (GFRP strips)"

Fig. 6 Prevalent failure mechanisms for examined slabs

(c) Flexural - rupture failure for slab (S-G-3STA)

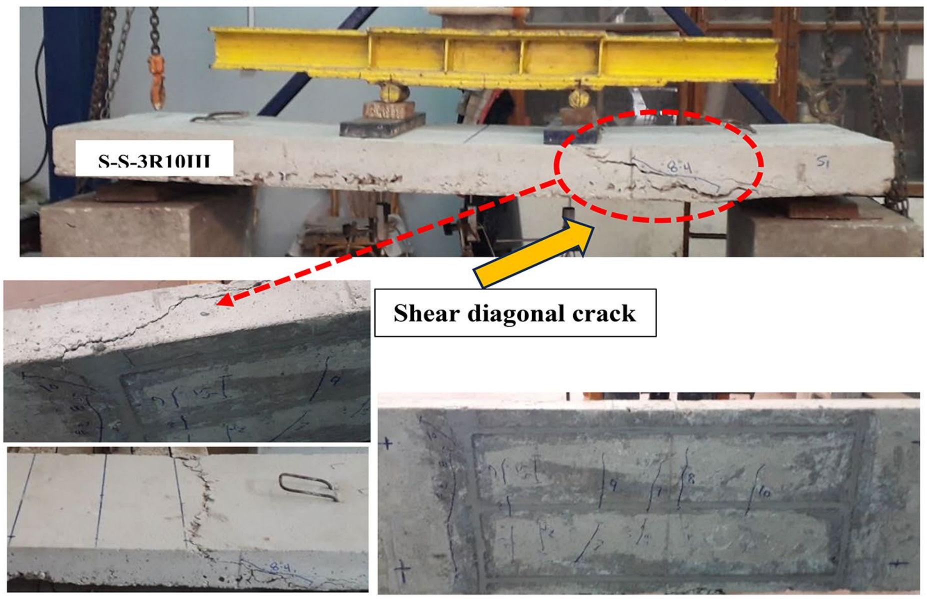

(d) Flexural-shear mode for slab (S-S-3R10III)

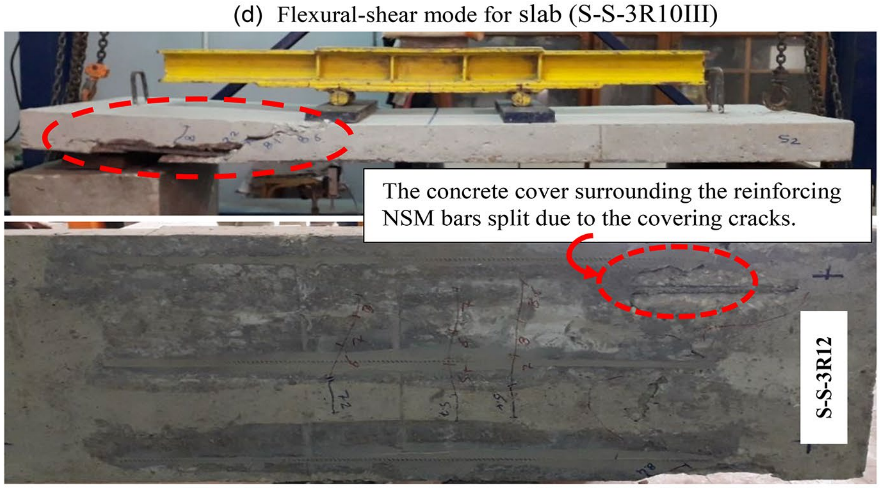

(e) Flexural – shear - debonding failure " flexural – shear, then de-bonding of the (NSM-bars)"

Fig. 6 continued

4.1.3 Flexural–Rupture Mode

This mode of failure was seen in Slab S-G-3STA, the GFRP strips ruptured when the de-bonding act started at the primary flexural split near the crucial region centrally located. Due to exposure to the overwork stress of significant cracks, the GFRP strips de-bonded. While the GFRP strips ruptured between the anchors, there was no sign of an anchor collapse, as shown in Fig. 6c.

4.1.4 Flexural–Shear Mode

In case the flexural strength is greater than the shear capacity, shear failure is the dominant failure. Three 10 mm NSM-steel bars with innovative end anchoring (III-shaped) were used for strengthening the slab (S-S-3R10III). Due to the inventive end anchoring, the NSM steel bars were effectively bonded to the RC slab. Because of this, the NSM bars acted as a single unit until an increased amount of loading. As anticipated, the flexural fractures initially appeared in the middle and spread toward the end, and the shear capacity was decreased, permitting the formation of shear cracks at the shear zone until full failure happened as illustrated in Fig. 6d.

4.1.5 Flexural–Shear–Debonding Mode

The NSM-bars method was used to test slabs with different materials, revealing identical cracks to the reference specimen. However, as load increased, more cracks appeared, causing flexural and shear failure. The composite behavior was not affected by de-bonding between concrete and epoxy or epoxy and NSM bar interfaces.

4.2 The Loads at 1st Cracking and Ultimate Capacities

The RC slabs that had been tested both with and without strengthening were visually observed until the initial crack was seen, at that point the associated carry (P_{cr}) was recorded. The observed loads for each tested slab are shown in Table 3 and Fig. 7 for both the maximum flexural and first-cracking timings. The reference slab displayed the smallest amount of the first crack load, and the percentage of the first crack's load to the total capacity was 55.5%. For the different strengthened slabs, the progression of loading at beginning cracking to maximum capacity ranged between 50% and 59.1. All strengthened slabs had greater loads at the first crack than the reference slab by varying values. The greatest percentage of the loads at the initial cracking to the pertinent failure load for slab S-S-3R10III was 59.1%. The loads at the first crack of slabs fortified employing the NSM technique were exceptional when compared to slabs strengthened utilizing the EB-system. That capability is related to the NSM technique's crack-arresting effectiveness, which altered the cracking pattern and exceeded the EB-system.

According to the reported results of the maximum load-carrying capacities for all slabs in Table 3 and Fig. 7, it is evident that the different strengthened slabs offered flexural ability (P_{ult}.) that was noticeably higher than that of the reference slab which was without any strengthening. These improvements in the maximum load for externally bonded technique-strengthened slabs were 73.3% and 91.1%, respectively, for the slabs S-G-3ST and S-G-3STA, showing the efficacy of using

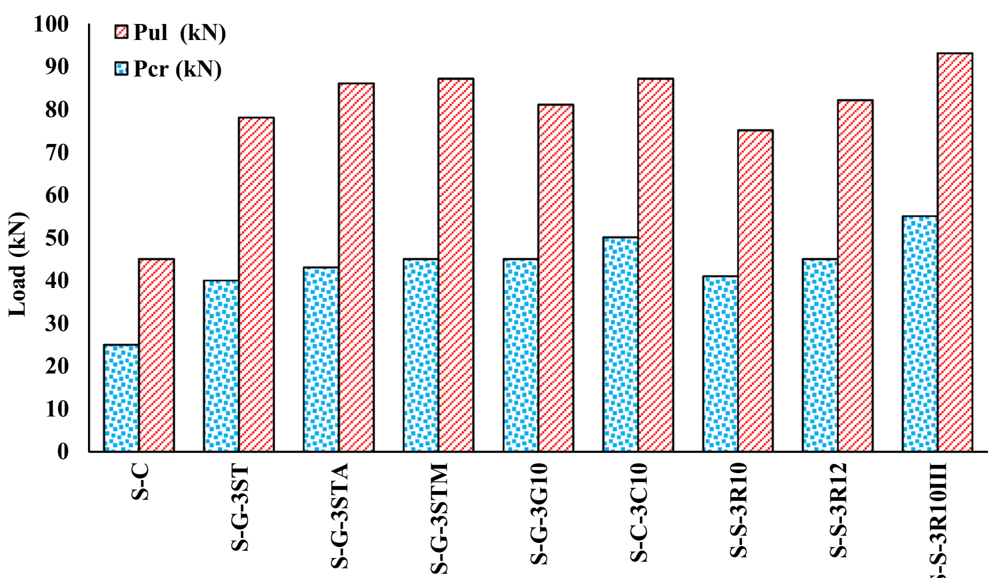

Fig. 7 First cracking and ultimate loads for all tested slabs

the proposed anchor mechanism for fiber strips as an enhancing method for one-way slabs. In order to explain the effectiveness of the novel EBECC system used to strengthen the S-G-3STM slab, the ultimate load improved by 93.3% in comparison to the control slab. Additionally, compared to the identical slab strengthened by the EB approach, it gave an increase of 11.6%.

In terms of the several material types used for NSM bars. The fiber carbon outperformed the glass fiber and steel in terms of ultimate load efficiency. They gave an increase by 7.5% more than NSM-GFRP bars and 16% more than NSM-steel bars-strengthened slabs, so, NSM-CFRP strengthened slab showed larger gain in P_{ul}. Regarding the amount of area steel, the RC slab that was strengthened by three steel rods that have a 12-mm size using the (NSM) approach had a capacity that was 9.33% greater than the slab that was strengthened by three steel rods with a size of 10 mm.

In terms of the ultimate load improvement, the slab strengthened with three III-shaped steel bars exhibited a higher improvement than the specimen fortified by a straight steel rods. It was shown that adding an anchor to the end of the NSM-bars as a enhancing system for reinforced concrete slabs worked well. The specimen strengthened with three steel rods in a III-shape had a 107% and a 24% superior strength compared to the control slab and the slab strengthened by straight bars with no ending fixings, respectively. We noted that the separating of the bars out the concrete groove caused the slab strengthened by straight bars to break even though the bar had not attained its overall tension strength. Markedly, the proposed end-anchor system for NSM bars had the excellent influnuce on the strengthening method.

4.3 Load–Deflection Relationships Based on Study Parameters

Comparing all strengthened RC slabs to the reference slab revealed a noticeable improvement in strength and stiffness. At the same loading stages, strengthened slabs showed lower deflection values than the control slab, as illustrated in Fig. 8a–e.

4.3.1 The Efficiency of the Suggested Anchoring Technique for EB-GFRP Strips

By observing the response of the slabs S-G-3ST and S-G-3STA, as demonstrated in Fig. 8a, it was possible to assess the impact of fortifying utilizing the proposed anchorage on the flexural characteristics of the examined slab strengthened by GFRP strips adopting the EB technique. By using GFRP strips with an anchor, the capacity increased (91.11%) against the control slab, and the deformation at the control slab's ultimate load was reduced by (65%). When GFRP strips were utilized without anchors, the capacity increased by 73.33% compared with the control slab, and the amount of displacement seen at the point of collapse of the reference slab decreased by nearly 60%. It is reported that using GFRP strips with an anchor improved the max strength by 10.3% compared to using GFRP strips without an anchor to reinforce the slab. Additionally, compared to the slab reinforced by the identical GFRP strips but no had an anchor, the suggested anchoring containing bundles of strands of glass fiber created a fan shape under the sheet increased the stiffness and rigidity. This is because the GFRP strips and concrete surfaces adhere to each other perfectly.

4.3.2 Influence of the Used Strengthening Systems

NSM, EB, and EBECC were the three strengthening methods utilized in this study, and it was possible to detect their effects on the behavior of the specimens under examination by seeing how the slabs in groups 2 and 3 performed after being strengthened. When compared to the control slab, using the externally bonded approach improved the ultimate load with ratios between 73.33 and 91.11% and reduced the deflection mentioned at the control specimen's failure load with a percentage between 60 and 65%. In comparison to the reference slab, the near-surface mounted system improved the final load by 67 to 107% while reducing the deformation of the reference slab at the final load by 65 to 79%. Comparing the EB to the NSM methodology, the EB technique produced lower capacities. Fixing an anchoring end to the NSM bars was found to be more successful than attaching an anchorage dowel to the EB sheet, can also be deduced.

It is achievable to illustrate the effect of the EBECC scheme on the performance of the specimens that were evaluated by analyzing the S-G-3ST and S-G-3STM slabs' efficiency for the strengthened slabs. The comparison of the load–deformation curves is shown in Fig. 8b. In comparison to the reference beam, the suggested EBIG system improved the result's capacity by 93.33%, and it reduced the deflection corresponding to the control specimen's ultimate load by a ratio of 70.83%. By applying the EB method to the same three GFRP strips, the capacity was increased by 73.33% comparatively to the reference slab, and the deflection mentioned at the control slab's maximum load capacity was decreased by 60%. The connection that exists across the slab's surface and the thin covering of grout is what gives the EBECC strengthening technique slab its better strength and stiffness over the slab strengthened using the EB technique.

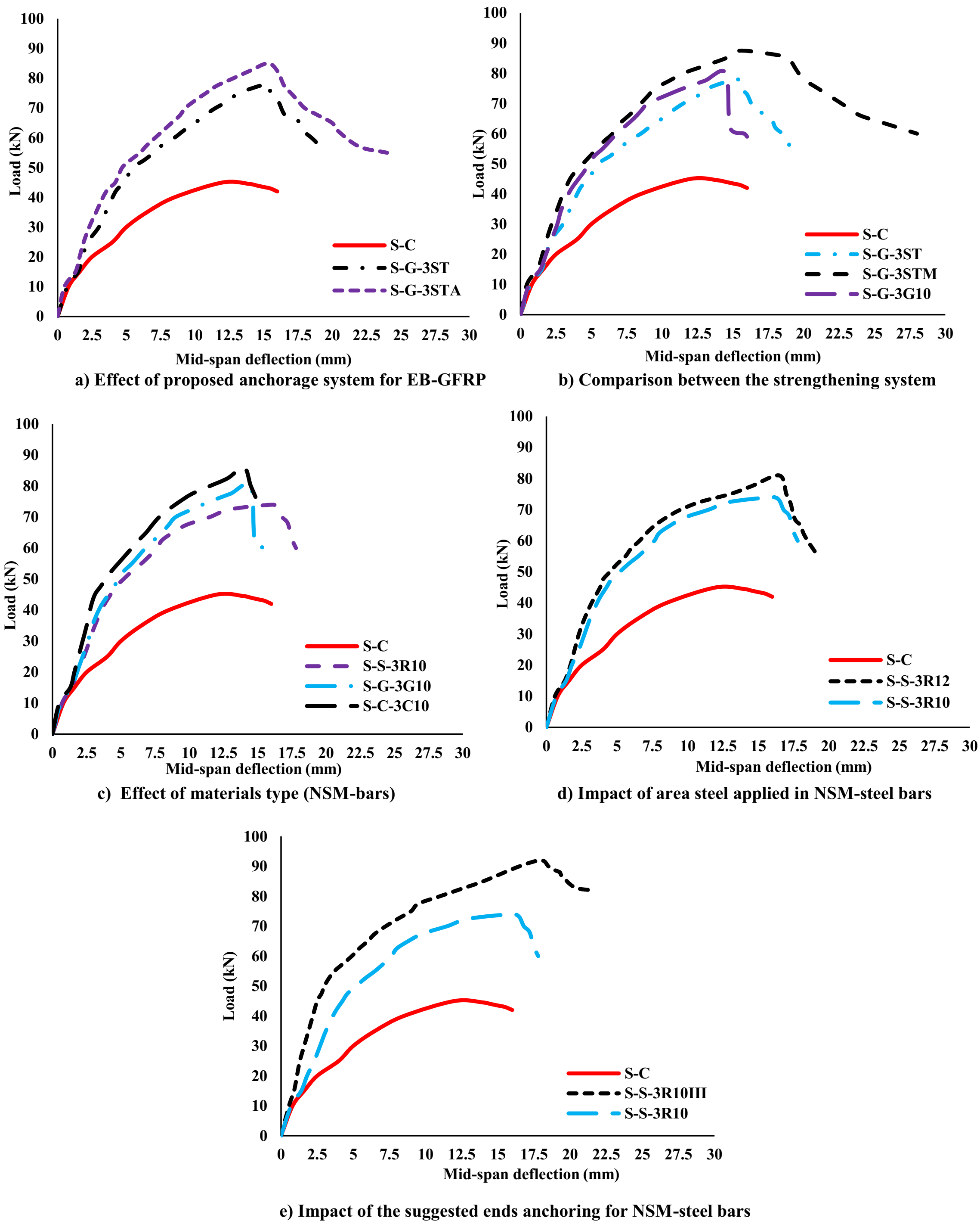

Fig. 8 Comparison among load–deflection curves

4.3.3 Effect of the Materials Used in NSM-bars

The outcomes of using several NSM bars for the strengthened slabs becomes readily noticeable in the slabs (S-C-3C10, S-G-3G10, and S-S-3R10). The influence of this variable on the flexural performance of tested slabs could be noticed, as illustrated in Fig. 8c. It is clear that the slab fortified by NSM-CFRP bars gives a maximum load capacity of 7.4% and 16% higher compared with slabs strengthened by glass fiber bars and steel bars, respectively, because of the superior strength of the carbon. Additionally, comparatively to slabs fortified with (GFRP) and (steel) NSM—rods, the slab strengthened by NSM-CFRP bars exhibited a significantly bigger stiffness because of a higher elasticity modulus. The highest metrics of deformation at failed for a slab strengthened with NSM steel bars are extremely useful since they demonstrate the improved ductility of the S-S-3R10 slab and provide an early warning of impending failure.

4.3.4 Impact of the Area Steel Used in NSM System

By investigating the structural characteristics of the slabs (S-S-3R10 and S-S-3R12) that were strengthened by three NSM-steel 10 mm and 12 mm size bars, respectively, it was possible to identify how the NSM area steel affected the structural performance of the examined specimens.

The load and deformation relationships for those slabs and the reference slab are presented in Fig. 8d for comparison. Utilizing 3R10 and 3R12 NSM steel bars increased capacity by 75% and 82%, respectively. By employing NSM-3R12 steel bars for reinforcement, the control slab's (S-C) deflection at failure was reduced by 68.33%, and by using NSM-3R10 steel bars for reinforcement, the control specimen's deflection at final load was decreased by 64.5%.

According to slabs strengthened with a 10 mm, 12 mm diameter of steel, the capacity increased as the quantity of steel increasing but not by an identical rate, the use of 12 mm diameter NSM-steel resulted in an ultimate load that was roughly 10% higher compared with slab strengthened by 10 mm diameter NSM-steel.

4.3.5 Effectiveness of Suggested End Anchors for NSM-Steel Bars

By assessing the structural behavior of the slabs S-S-3R10III and S-S-3R10 that were strengthened using the NSM system, the effectiveness of the suggested ending anchoring of the near-surface mounted-steel bars may be observed. As illustrated in Fig. 8e, the relationships between load against deflection at the middle of the span were examined. The three NSM-steel bars with end anchors (III—formed) greatly increased the strength comparatively to the control slab (107%), and they also decreased the control slab's deformation at the final load by as much as 79.2%. When comparing to the reference slab, the max capacity increased by 66.7% when using NSM steel bars that are straight and have no ending anchors, and the deflection recorded during the S-C "reference slab" collapse, decreased with 64.6%. It may be determined that the suggested anchorage at the endpoints for bars resulted in a higher max capacity load by 24% approximately when comparable with a slab that has straight steel bars but no ending anchors. The NSM-steel bars' strong adhesion to the surface of the concrete is what gives them their distinguishing distinction. Comparing the slab with ending anchoring to the one without showing an increase in strength, ductility, and stiffness.

4.4 Ductility Indices (DI)

Ductility is attributed to the capacity of a material to undergo substantial inelastic deformations prior to failure. Ductility could be measured with ductility index (DI) which represents the ratio between the ultimate displacement to the yield displacement (Abdel-Karim et al., 2023). Ductility indices are reported in Table 3 and Fig. 9.

In comparison to another specimens, the specimen strengthened using the EBECC approach performed better in terms of ductility. The slabs enhanced with CFRP NSM bar and GFRP NSM bar displayed lower ductility indices compared to differently fortified slabs because both carbon fiber and glass fiber are more brittle.

5 Energy Absorption (E_{tot})

Energy absorption capacity is defined by the area under the load–deflection curve (Abdel-Karim et al., 2023). The calculated energy absorption of all tested specimens is presented in Table 7. It is reported that strengthening techniques help in improving energy absorption in the range of 57% to 352% when compared with control specimen. This could be owing to the effectiveness of the novel techniques in the application of RC slabs strengthening.

6 Stiffness

To calculate the ultimate stiffness (Ku) and uncracked stiffness (Ki) for each of the examined slabs, the displacement and loading values at the final and cracking situations, respectively, are displayed in Table 3 and Fig. 10. It depicts that, as compared to control slab, Ku and Ki significantly increased for the strengthened slabs, increasing by a range of 26 to 75% and 60 to 138%, respectively. In comparison to the reference specimen, the strengthened slabs showed better stiffness when taking the effect of strengthening into account. The findings showed that Ku was less impacted than Ki.

7 Analytical Study

According to the formula $0.5P_u{*}X$, where X is the flexural span of 0.50 m and $P_{ul.}$ is the ultimate load, the experimental moment for each slab was determined. According to limiting condition rules, which demand that the internal forces equilibrium and strain integration be fulfilled on every cross-section, the design conditions of the examined slabs were created. On the belief that FRP would experience a linearly elastic stress–strain curve until collapse and that

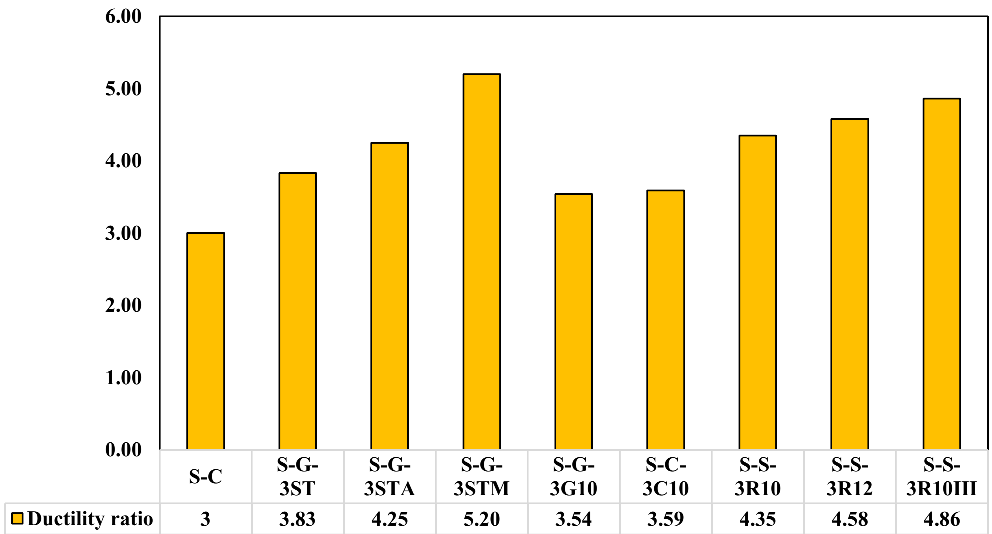

Fig.9 Ductility ratio comparison for all tested slabs

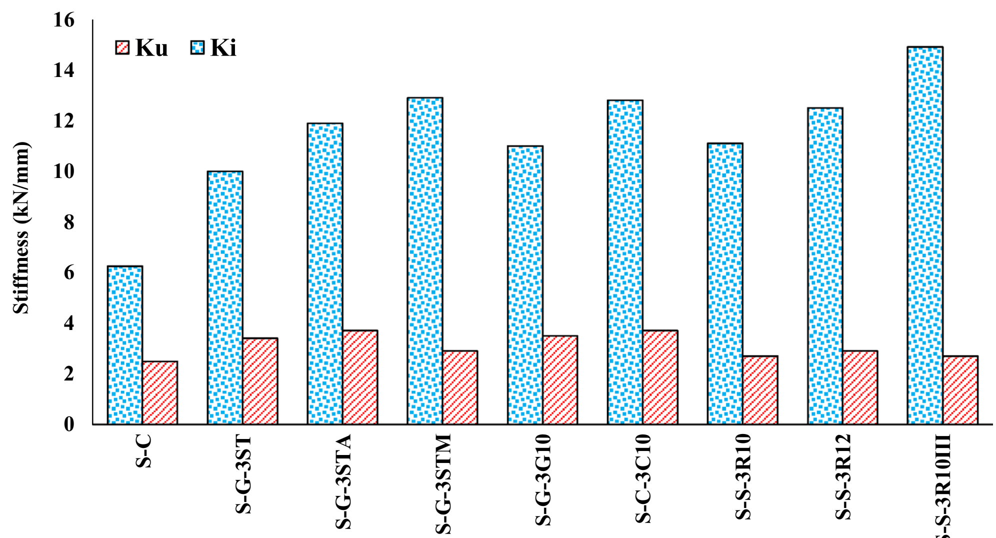

Fig. 10 Stiffness comparison for all tested slabs

there will be no corresponding slipping in between fiber and concrete, NSM bars or EB sheets are used as supplementary fortification with various material qualities. ACI 440-2R-17 (ACI, 2017), and Abdulrahman, B.Q. and Aziz, O.Q. (Bassam Qasim Abdulrahman, 2021) were applied to determine the tested slabs capacities, which were then compared to the maximum load suggested by the testing findings. The following lists the calculations and equations that were used:

– Calculating the strain on the outer face (ε_{bi}) of the beam using Eq. (1)*:*

$$\varepsilon_{bi} = \frac{M_{bi}(d - k\,d)}{I_{cr}E_c} \tag{1}$$

– Let us assume that, as a first approximation, the distance measured (c) from the neutral axis to the compression fiber is equal to 0.15 of the slab's actual thickness (d). The value is then changed after making sure that internal forces are in equilibrium.
– Using Eqs. (2) and (3), calculate the strains for both RC section and the fiber strengthening item:

$$\varepsilon_c = \left(\varepsilon_{fe} + \varepsilon_{bi}\right)\left(\frac{c}{d_b - c}\right), \quad (2)$$

$$\varepsilon_{fe} = 0.003\left(\frac{d_b - c}{c}\right) - \varepsilon_{bi} \quad (3)$$

– The greatest value, as specified by ACI 318-05, is ε_c= 0.003. The principal reinforcement steel of the strain of the slab ε_s, created by Eq. 4, was recognized:

$$\varepsilon_s = (\varepsilon_{fe} + \varepsilon_{bi})(\frac{d - c}{d_f - c}) \quad (4)$$

– Using Eqs. (5) and (6) to identify the stresses in the fiber and the reinforcement steel:

$$f_s = E_s\,\varepsilon_s \le f_y, \quad (5)$$

$$f_{fe} = E_f\,\varepsilon_{fe} \quad (6)$$

– Using Eq. 7 to calculate the resultant straining actions and validate the equilibrium:

$$c = \frac{A_s f_s + A_f f_b}{\alpha_1 f_c'\,\beta_1\,b} \quad (7)$$

– For the final failure brought on either FRP rupture or FRP debonding, the terms _ α_1 and β_1 in Eq. (7) must be calculated from the parabolic stress–strain equation for concrete and are represented as in Eqs. The technique was iterative, and the c value was changed if the straining actions results did not match:

$$\alpha_1 = \frac{3\,\varepsilon'_c\,\varepsilon_c - {\varepsilon_c}^2}{3\,\beta_1\,\varepsilon'^2_c} \quad (8)$$

$$\beta_1 = \frac{4\varepsilon_c^{'} - \varepsilon_c}{6\,\varepsilon_c^{'} - 2\,\varepsilon_c} \quad (9)$$

where $\varepsilon_c^{'} = \frac{1.7f_c^{'}}{E_c}$.

– Calculating the flexural capacities using Eqs. (10-12):

$$M_{ns} = A_s f_s\,(d - \frac{\beta_1\,C}{2}) \quad (10)$$

$$M_{nf} = A_f\,f_{fe}\left(d_b - \frac{\beta_1\,C}{2}\right) \quad (11)$$

$$M_{total} = M_{ns} + \varphi_f M_{nf} \quad (12)$$

The findings from the investigation and analytical study are listed in Table 4. Fig. 11 compares the projected ultimate load values for all tested slabs to the observed values in accordance with Table 4. The flexural capabilities of each strengthened slab were predicted by the ACI 440-2R-17 to be within tolerable bounds.

8 Finite Elements Investigation

In this section, the experimental results for the tested one-way RC slabs in this research are validated using the nonlinear tool for finite element modeling Abaqus/CAE version 6.14-2 (ABAQUS, 2014; Bassam Qasim Abdulrahman, 2022). Numerical simulation was performed using explicit FE solver. Comparative analysis was done between the experimental results and the numerical outcomes of this simulations, which included all tested slabs. The configuration of FEA models is shown in Figs. 11 and 12. The FEA study specifics are listed in the following sections.

8.1 Geometry Modeling and Meshing

The concrete was modeled using a three-dimensional solid element (C3D8R), steel bars and stirrups were modeled with truss element (T3D2) and the supporting and loading plates were modeled using a rigid element. In addition, GFRP, and CFRP laminates were modeled using 3D deformable wire components (S4R). In FE, choosing the mesh density is a crucial step. The mesh size used in this investigation was 20 mm in all dimensions. A perfect bond between embedded steel and concrete was assumed. This perfect bond has been defined using embedded interaction between steel and concrete. The bond between the CFRP, GFRP and concrete was modeled using cohesive elements (COH3D8) with the adhesive layer being modeled using a single layer of cohesive elements (Bassam Qasim Abdulrahman, 2022). Debonding of the CFRP strips is represented by the onset of damage in the cohesive elements. Damage initiation is defined using a maximum nominal stress criterion as described by Smith et al. (2011).

8.2 Materials Modeling

8.2.1 Concrete Behavior Modeling in Compression

The parameters definition of the concrete damage plasticity (CDP) model for concrete were based on the developed equations by Zainal et al. (Iqbal et al., 2020) and are depicted in Fig. 13. The following equations were used to determine these parameters:

$$\sigma_c = (1 - d_c)E_0\left(\varepsilon_C - \varepsilon_C^{pl,h}\right) \quad (13)$$

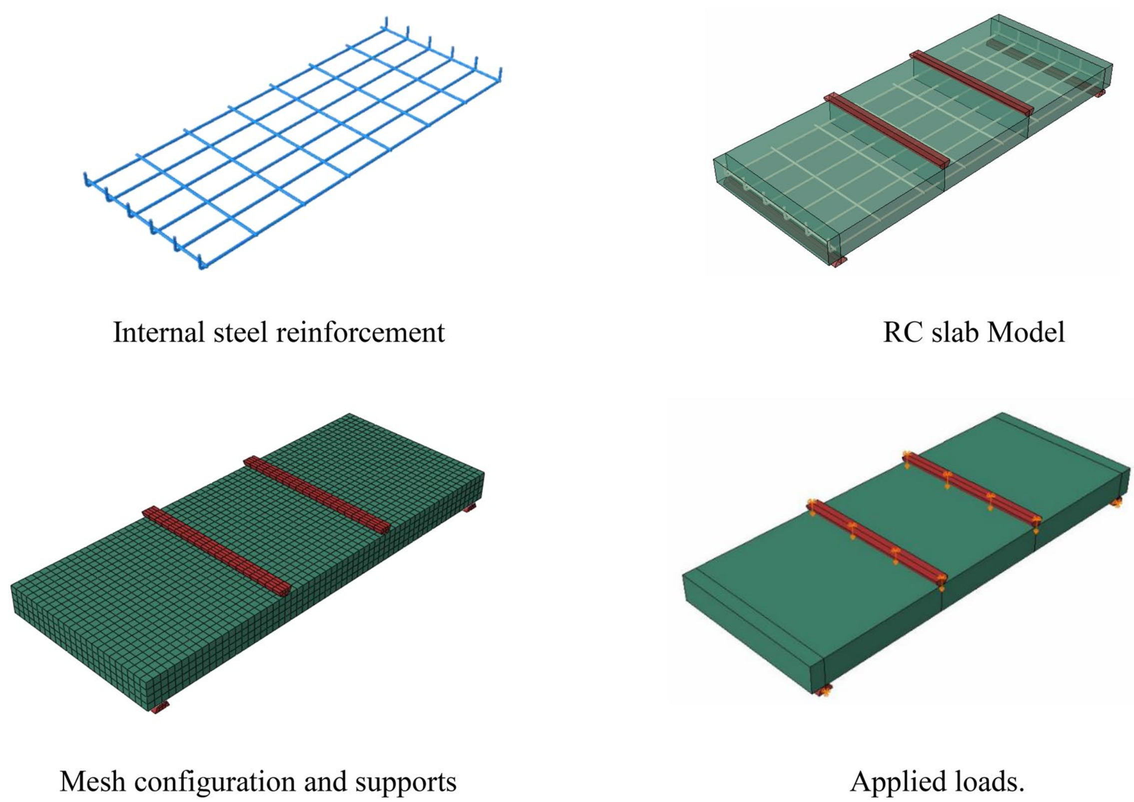

Fig. 11 Simulating RC one-way slab

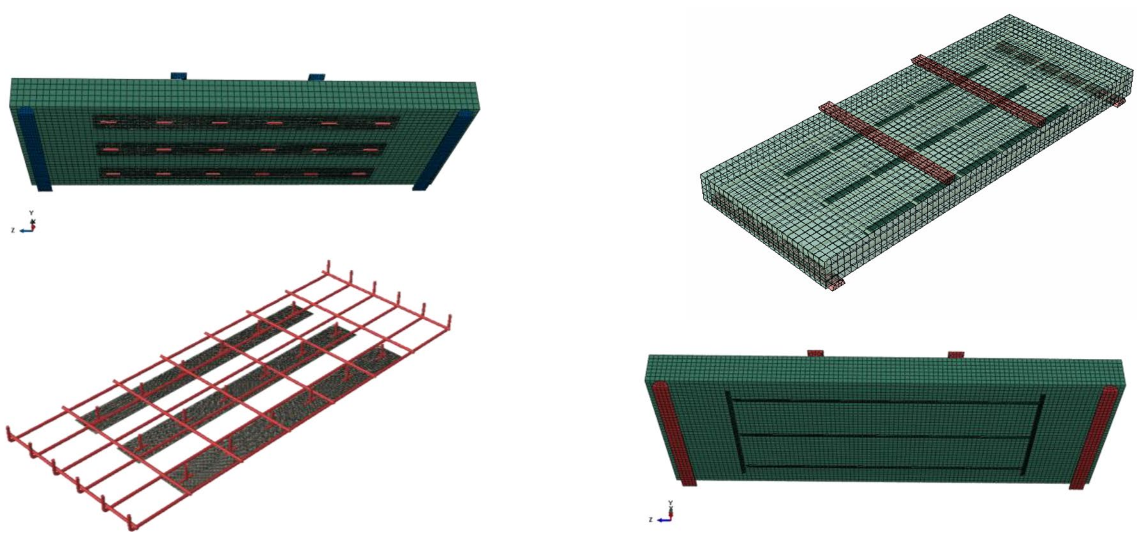

Fig. 12 Simulating of strengthening system of some slabs

$$\varepsilon_C^{in,h} = \varepsilon_C - \frac{\sigma_C}{E_O} \tag{14}$$

$$\varepsilon_C^{pl,h} = \varepsilon_C - \frac{\sigma_C}{E_O}\left(\frac{1}{1-d_c}\right), \tag{15}$$

$$\varepsilon_C^{pl,h} = \varepsilon_C^{in,h} - \frac{\sigma_C}{E_O}\left(\frac{d_c}{1-d_c}\right) \tag{16}$$

Furthermore, in this study, Kent and Park (Abdel-Karim et al., 2023) described the model for unconfined

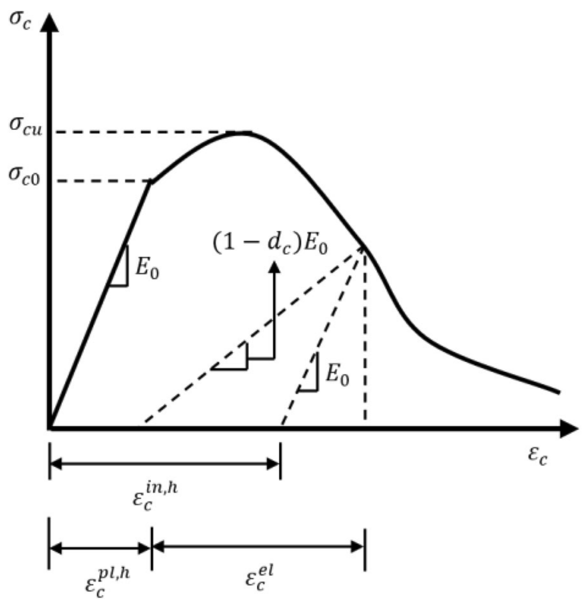

Fig. 13 Definition of concrete behavior for CDP model in compression

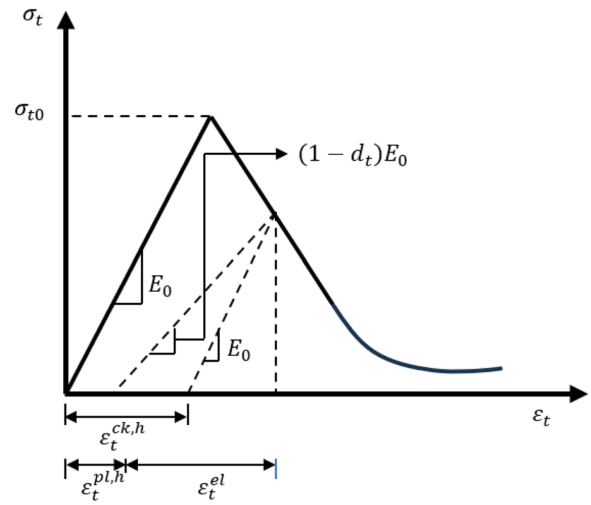

Fig. 14 Definition of concrete behavior for CDP model in tension

concrete behavior. This model is commonly represented by the following equation:

$$`\sigma_c = \sigma_{cu}\left[2\left(\frac{\varepsilon_c}{\varepsilon_c^{'}}\right) - \left(\frac{\varepsilon_c}{\varepsilon_c^{'}}\right)^2\right] \tag{17}$$

where σ_c and σ_{cu} are the nominal and ultimate compressive stress, ε_c and $\varepsilon_c^{'}$ are the nominal and ultimate compressive strain, respectively, E_o is the modulus of elasticity, $\varepsilon_C^{in,h}$ the elastic hardening strain in compression, and $\varepsilon_C^{pl,h}$ is the plastic hardening strain in compression.

The computation of compression damage parameter, d_c, may be achieved using the below equation:

$$d_c = 1 - \frac{\sigma_c}{\sigma_{cu}} \tag{18}$$

8.2.2 Concrete Behavior Modeling in Tension

The uniaxial tensile stress–strain behavior of concrete is simulated with Zainal et al. model (Iqbal et al., 2020), which is depicted in Fig. 14. The plasticity hardening strain in tension, $\varepsilon_t^{pl,h}$, is determined based on the following equations:

$$\sigma_t = (1-d_t)E_0\left(\varepsilon_t - \varepsilon_t^{pl,h}\right) \tag{19}$$

$$\varepsilon_t^{ck,h} = \varepsilon_t - \frac{\sigma_t}{E_O} \tag{20}$$

$$\varepsilon_t^{pl,h} = \varepsilon_t - \frac{\sigma_t}{E_O}\left(\frac{1}{1-d_t}\right) \tag{21}$$

$$\varepsilon_t^{pl,h} = \varepsilon_C^{ck,h} - \frac{\sigma_t}{E_O}\left(\frac{d_t}{1-d_t}\right) \tag{22}$$

where σ_t and σ_{to} are the nominal and ultimate tensile stress, ε_t is the nominal and ultimate compressive strain, respectively, E_o is the modulus of elasticity, $\varepsilon_t^{ck,h}$ the elastic hardening strain in tension, and $\varepsilon_t^{pl,h}$ is the plastic hardening strain in tension.

The models computed the tensile strength σ_{t0} equal to 7–10% of maximum compressive strength σ_{cu}. The tensile damage could be expressed as follows:

$$d_t = 1 - \frac{\sigma_t}{\sigma_{to}} \tag{23}$$

8.2.3 Steel Bars

The steel in the analysis is assumed to follow an ideal elasto-plastic constitutive model. It is assumed that there is a complete bond between steel and concrete. The steel support plates are treated as linearly elastic, meaning their behavior is assumed to be within the elastic range.

8.2.4 FRP Bars and FRP Sheets

The tensile behavior of FRP bars and sheets is characterized by an elastic material response. It follows a linear response until reaching the tensile strength or rupture strain, after which tensile failure occurs. Poisson's ratio of 0.3 was assigned to FRP.

8.3 Evaluation of the Computational Models

The results of the nonlinear finite element analysis (NLFEA) are in agreement comparing the results of the experiment evaluation of the tested one-way slabs, as shown in Fig. 15. Also, the development and deformation form of the FEM produced by ABAQUS are in good accord with the experimental performance, as shown in Fig. 16. Table 8 compares the FEM and experimental ultimate loads. The difference between the experimental and FEA maximum load ratios ranged from 1.01 to 1.09. It can be observed that ABAQUS predicts ultimate load than the load that was measured during the testing with very high accuracy. This comparison shows that when identical findings were obtained, experimental work, and FEA exhibited good agreement. Nevertheless, while the outcomes for the initial cracking load, final load, and deflection are satisfactory, the load–deflection curve revealed variations near failure. Fig. 17 compares experimental and FEM results for each slab's load vs mid-span deflection.

9 Conclusions

The flexural achievement of reinforced concrete slabs that had been strengthened with a variety of methods and materials were examined. Considering the experimental results, comparison with the NLFEA, and analytical flexural capacities in this paper, the next findings were reached:

1- The flexural load capacity for the tested slabs was improved by various strengthening techniques and materials by 67–107%.
2- The significant impact of the suggested end anchoring for NSM-steel bars, which provided the greatest structural strength and displayed most ductile index. This emphasized superiority is a result of the NSM-steel bars' strong adhesion to the concrete surface.
3- When compared to a slab strengthened by the identical GFRP strips but without an anchor, the anchoring for the EB-GFRP strips increased the ultimate resistance, stiffness, and ductility.
4- The influence of NSM-steel bars on flexural characteristics in comparison to the control slab, showed that using the three 10 mm or 12 mm diameter NSM steel bars increased the capacity by 67% and 83%, respectively. This shows that increasing the area of steel reinforcement by about two times did not enhance the final capacity by the same ratio.
5- The NSM-CFRP bars-enhanced slab had a larger capacity than the steel and GFRP-enhanced slabs, however, that slab it a highly brittle behavior at failure.

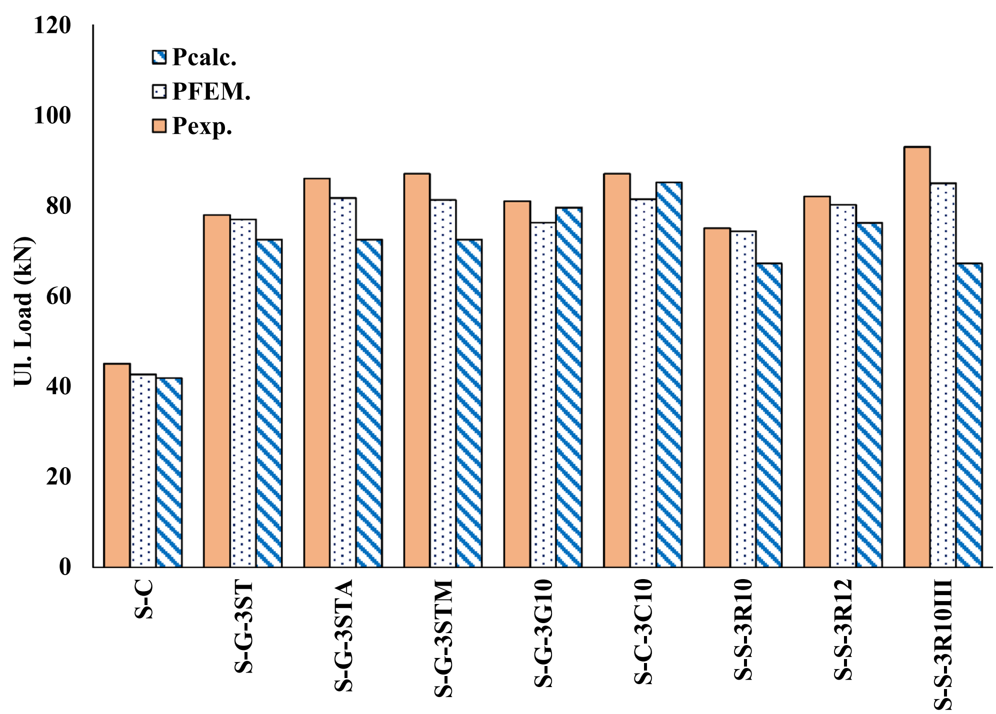

Fig. 15 For all slabs, a comparison of experimental, calculated, and FEM ultimate loads

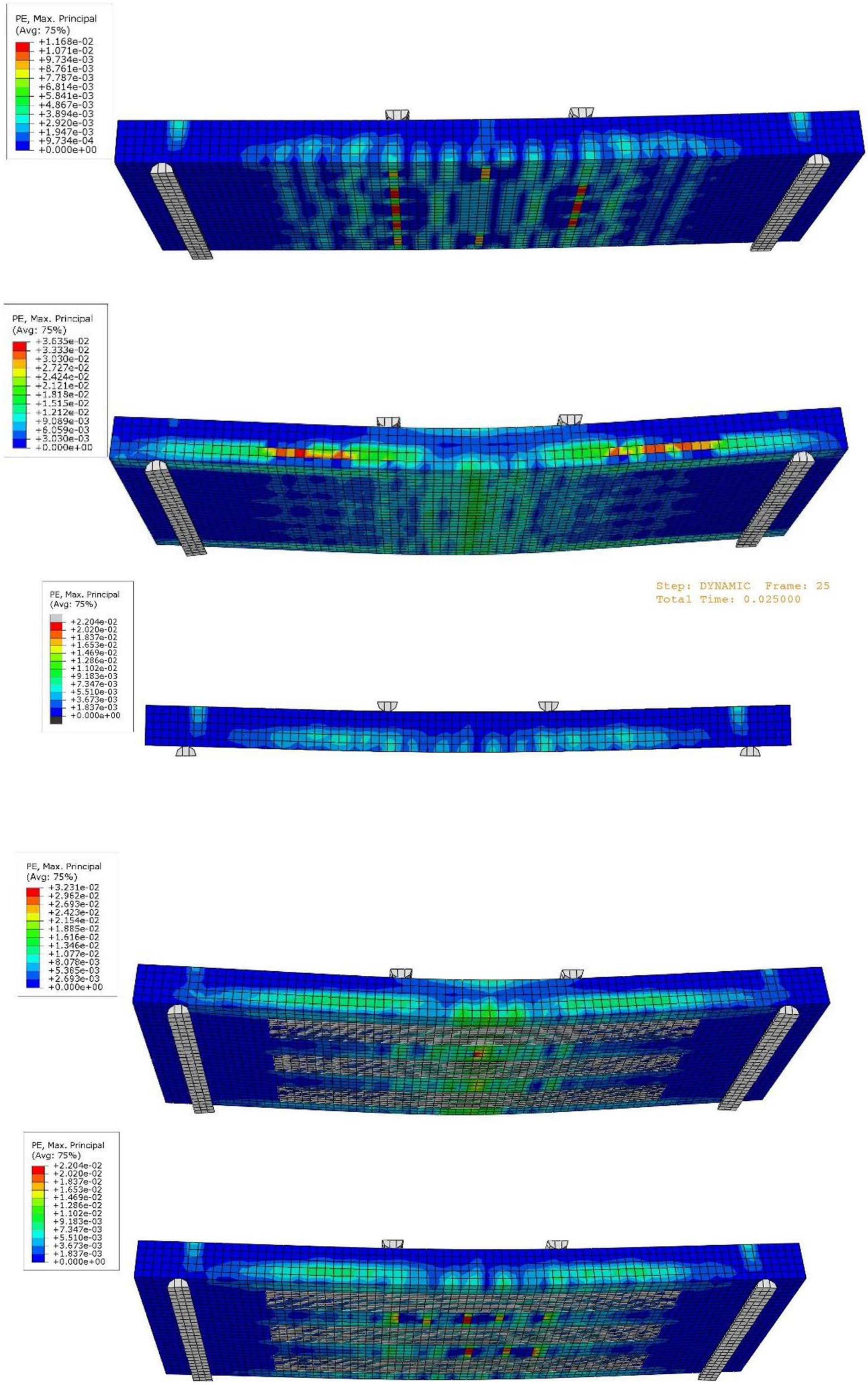

Fig. 16 Progression of cracks at failure for some slabs

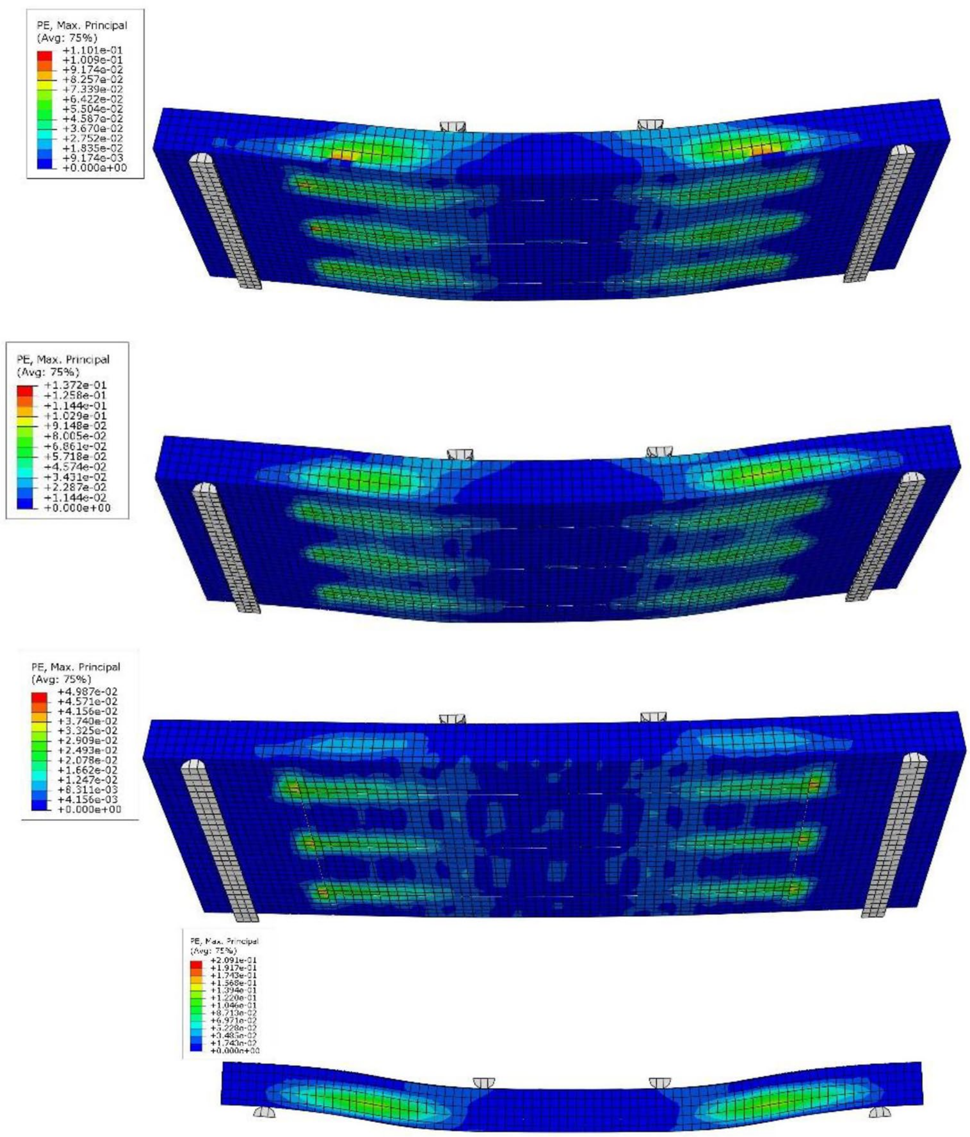

Fig. 16 continued

Table 8 Results for the maximum loads from the analytical and NLFEA are compared with those from the tests

Slabs name	Ult. loads (kN)		$P_{exp.}/P_{calc}$	Ult. loads (kN)		$P_{ex.}/P_{FEA}$
	P_{ex}	P_{cal}		P_{ex}	P_{FEA}	
S-C	45	41.9	1.07	45	42.7	1.05
S-G-3ST	78	72.5	1.08	78	76.9	1.01
S-G-3STA	86	72.5	1.19	86	81.7	1.05
S-G-3STM	87	72.5	1.20	87	81.3	1.07
S-G-3G10	81	79.5	1.02	81	76.3	1.06
S-C-3C10	87	85.1	1.02	87	81.5	1.07
S-S-3R10	75	67.2	1.12	75	74.3	1.01
S-S-3R12	82	76.2	1.08	82	80.2	1.02
S-S-3R10III	93	67.2	1.38	93	85	1.09
Average			1.12			1.04

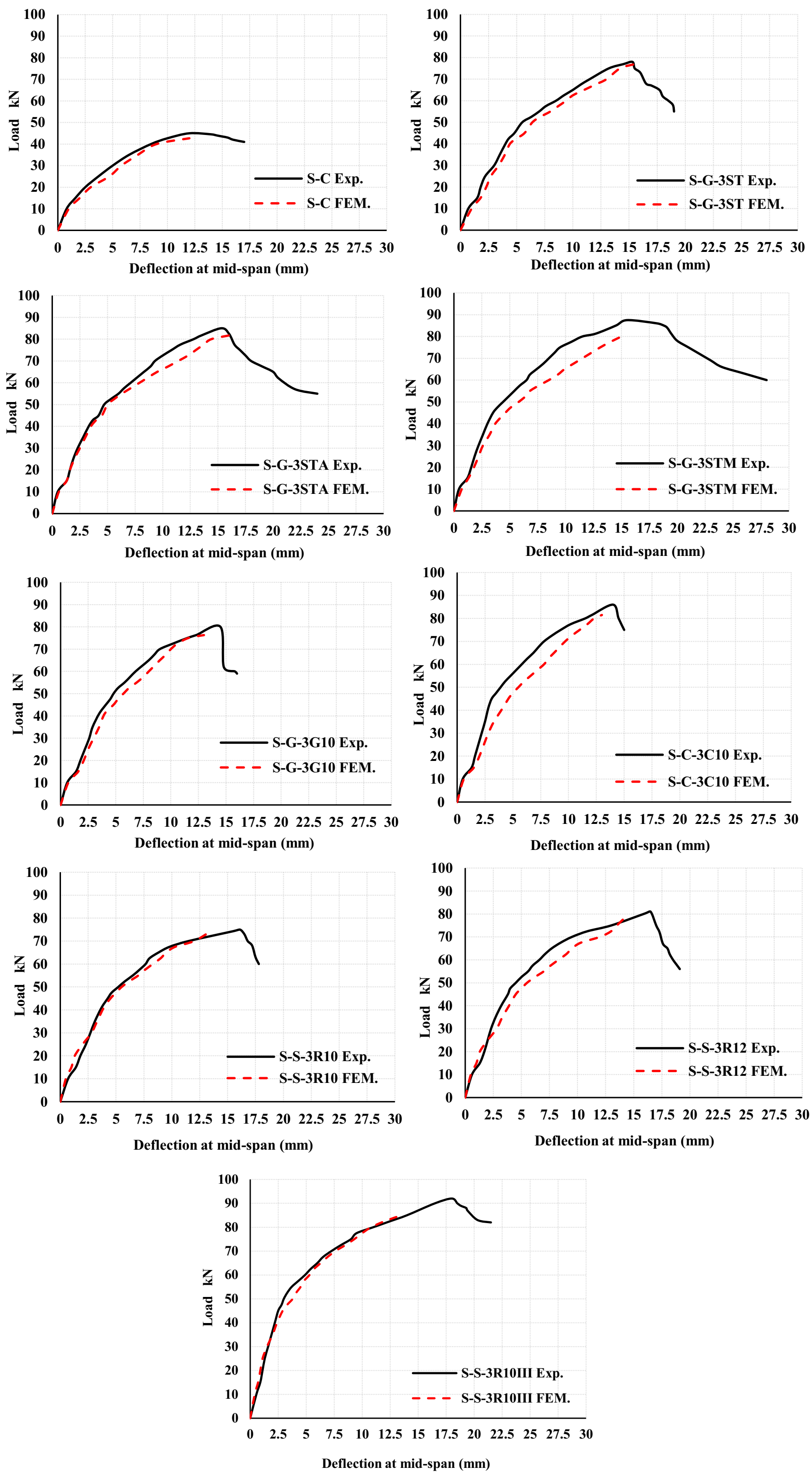

Fig. 17 Experimental and FEM (load versus. deflection) relations are compared

6- When compared to specimens strengthened with GFRP, and CFRP NSM bars, that slab strengthened with NSM-steel bars showed a significantly greater deformation at failure. That is because they demonstrate the particularly ductile nature of utilizing steel bars in the NSM strengthening process. The high displacement values at failure provided a significant advantage by providing an indication prior to failure.
7- Higher ultimate strength and stiffness were obtained when utilizing the EBECC methodology compared to this slab strengthened using the EB methodology. That supremacy is related to the perfect adhesion of the concrete surface and the thinner mortar covering. So, the novel strengthening technique is highly recommended for enhancing the flexural capacity of one-way slabs.
8- The displayed capacities of the tested slabs using the ACI 440 equations were reasonable and conservative having a mean percentage of 10% when viewed alongside the results of the testing.
9- ABAQUS is capable of simulating and analyzing strengthened slabs as a nonhomogeneous material with a nonlinear response and produces satisfactory results.
10- The numerical capacities, which ranged from 1.01 to 1.09, closely matched the experimental findings, and the load–deformation relations from FEA exhibited a linear relationship up to fracture load, which roughly corresponds to the true values.

List of symbols

A_s Area of steel reinforcement
A_f FRP area (bars or strips)
c A distance between the compressed edge and neutral axes
d Space between the external compressive surface and the CL of the bottom inner reinforcement
d_b Effective thickness to sheets of NSM-RMF or EB-FRP
E_c Concrete elasticity modulus
E_f Modulus elasticity of fiber
E_s Steel elasticity modulus
f_c' The specified compression strength of RC
f_{fe} Actual stress in fiber sheets or bars at fail
f_{fu} Calculate the maximum tensile strength of fiber.
f_s Reinforcing steel stress
f_y Yield stress
I_{cr} Cracked inertia
K The ratio of reinforcing depth is determined by comparing the distance of the equilibrium axis to the severe compressive surface
α_1 A factor that is used to determine the concrete's corresponding rectangular stress distribution.
β_1 The proportion of a rectangular stress block's depth to its associated neutral line height
ε_{bi} At the time of installing the reinforcement bars, the concrete substrate was under strain.
ε_c Strain of concrete
ε_c' Maximal strain of unconfined RC corresponding to f_c'
ε_{fe} Attained efficient strain levels in NSM bars or fiber sheets.
ε_{fu} Design rupture strain of fiber rods or sheets.
φ_f Fiber strength reduction factor = 0.85 (under flexure)
F-M Normal–flexural mode.
F-D-M Flexural–debonding mode
F-R-M Flexural–rupture mode
F-S-M Flexural–shear mode
F-S-D-M Flexural–shear–debonding mode

Acknowledgements
Not applicable.

Author Contributions
M.H.M: designed the experimental program methodology, performed the experimental program methodology, investigation, and original draft. I.A.E: numerical modeling, review and editing. M.M: numerical modeling, review and final draft. All authors read and approved the final manuscript.

Funding
Open access funding provided by The Science, Technology & Innovation Funding Authority (STDF) in cooperation with The Egyptian Knowledge Bank (EKB). Not applicable.

Availability of Data and Materials
All data generated or analyzed during this study are included in this published article.

Declarations

Competing Interests
There is no competing interest associated with the submission of this manuscript.

Received: 2 December 2023 Accepted: 27 March 2024
Published online: 26 July 2024

References

ABAQUS, (2014) Abaqus/CAE 6.14 User's Manual, Dassault Syst´emes Inc. Provid. RI, USA. IV.
Abdel-Karim, A. H., Khalil, G. I., Ewis, A. E., & Makhlouf, M. H. (2023). Impact of developed hybrid polypropylene fiber inclusion on the flexural performance of concrete beams reinforced with innovative hybrid bars. *Construction and Building Materials, 409*, 134113.
Abdulrahman, B. Q. (2022). Precise finite element verification of the unreliability of using multi-layers of FRP on CFRP-debonding in RC beams. *Engineering Research Express, 4*(2), 025048. https://doi.org/10.1088/2631-8695/ac7945
Abdulrahman, B. Q., & Aziz, O. Q. (2021). Strengthening RC flat slab-column connections with FRP composites: A review and comparative study. *Journal of King Saud University (engineering Sciences), 33*, 471–481. https://doi.org/10.1016/j.jksues.2020.07.005
ACI 440.2R-17, (2017) Guide for the Design and Construction of Externally Bonded FRP Systems for Strengthening Concrete Structures, American Concrete Institute, Farmington Hills, Mich, USA
Afefy, H. M., & Fawzy, T. M. (2013). Strengthening of RC one-way slabs including cut-out using different techniques. *Engineering Structures*. https://doi.org/10.1016/j.engstruct.2013.09.013
Ali, T., & Yehia, S. (2016). Study on strengthening of RC slabs with different innovative techniques. *Open Journal of Civil Engineering, 6*(04), 516.
Al-Obaidi, S., Saeed, Y. M., & Rad, F. N. (2020). Flexural strengthening of reinforced concrete beams with NSM-CFRP bars using mechanical interlocking. *Journal of Building Engineering*. https://doi.org/10.1016/j.jobe.2020.101422
Amin, M. N., Khan, K., et al. (2022). Investigating the bond strength of FRP rebars in concrete under high temperature using gene-expression programming model. *Polymers*. https://doi.org/10.3390/polym14152992
Anil, Ö., Kaya, N., & Arslan, O. (2013). Strengthening of one-way RC slab with opening using CFRP strips. *Construction and Building Materials, 48*, 883–893.

Barris, C., Sala, P., Gómez, J., & Torres, L. (2020). Flexural behaviour of FRP reinforced concrete beams strengthened with NSM CFRP strips. *Composite Structures*. https://doi.org/10.1016/j.compstruct.2020.112059
Choi, K. S., Lee, D., You, Y. C., & Han, S. W. (2022). Long-term performance of 15-year-old full-scale RC beams strengthened with EB FRP composites. *Composite Structures*. https://doi.org/10.1016/j.compstruct.2022.116055
Correia, L., Sena-Cruz, J., Michels, J., França, P., Pereira, E., & Escusa, G. (2017). Durability of RC slabs strengthened with prestressed CFRP laminate strips under different environmental and loading conditions. *Composites Part b: Engineering, 125*, 71–88.
De Lorenzis, L., & Teng, J. G. (2007). Near-surface mounted FRP reinforcement: An emerging technique for strengthening structures. *Composites Part b, Engineering, 38*, 119–143.
El-Gamal, S. E., Al-Nuaimi, A., Al-Saidy, A., & Al-Lawati, A. (2016). Efficiency of near surface mounted technique using fiber reinforced polymers for the flexural strengthening of RC beams. *Construction and Building Materials, 118*, 52–62.
El-Mandouh, M. A., Elsamak, G., Rageh, B. O., & Hamoda, A. (2023). Experimental and numerical investigation of one-way reinforced concrete slabs using various strengthening systems. *Case Studies in Construction Materials*. https://doi.org/10.1016/j.cscm.2022.e01691
El-Mandouh, M. A., Hu, J. W., Shim, W. S., Abdelazeem, F., & ELsamak, G. (2022). Torsional improvement of rc beams using various strengthening systems. *Buildings, 12*, 1776. https://doi.org/10.3390/buildings12111776
Elsanadedy, H. M., Almusallam, T. H., Alsayed, S. H., & AL-Salloum, Y. A. (2015). Experimental and FE study on RC one-way slabs upgraded with FRP composites. *KSCE Journal of Civil Engineering*. https://doi.org/10.1007/s12205-013-0689-y
ELWakkad, N. Y., Heiza, K. M., Tayeh, B. A., & Mansour, W. (2023). Experimental study and finite element modelling of the torsional behavior of self-compacting reinforced concrete (SCRC) beams strengthened by GFRP. *Case Studies in Construction Materials, 18*, e02123. https://doi.org/10.1016/j.cscm.2023.e02123
Fernandes, H., Lúcio, V., & Ramos, A. (2017). Strengthening of RC slabs with reinforced concrete overlay on the tensile face. *Engineering Structures, 132*, 540–550.
Galati, D., & De Lorenzis, L. (2009). Effect of construction details on the bond performance of NSM FRP bars in concrete. *Advances in Structural Engineering, 12*(5), 683–700.
Hu, B., Zhou, Y., Xing, F., Sui, L., & Luo, M. (2019). Experimental and theoretical investigation on the hybrid CFRP-ECC flexural strengthening of RC beams with corroded longitudinal reinforcement. *Engineering Structures*. https://doi.org/10.1016/j.engstruct.2019.109717
Iqbal, S. M., Zainal, S., Hejazi, F., Abd Aziz, F. N. A., & Jaafar, M. S. (2020). Constitutive modeling of new synthetic hybrid fibers reinforced concrete from experimental testing in uniaxial compression and tension MDPI. *Cryst, 10*, 885.
Khalil, A. E. A., Atta, A. M., Hassan, A., & Abd-Elaaty, A. H. (2022a). Flexural strength recovery of RC one-way slabs having cut-outs using NSM-SHCC plates. *Engineering Structures, 258*, 114149.
Laraba, A., Merdas, A., Chikh, N.E. (2014). Structural performance of RC beams strengthened with NSM CFRP. In: Proceeding of the World Congress on Engineering, vol. II, London, 978–988, 2014.
Makhlouf, M. H., Ismail, G., Kreem, A. H. A., & Badawi, M. I. (2023). Investigation of transverse reinforcement for RC flat slabs against punching shear and comparison with innovative strengthening technique using FRP ropes. *Case Studies in Construction Materials*. https://doi.org/10.1016/j.cscm.2023.e01935
Makhlouf, M. H., & Mansour, M. H. (2023). Efficiency of innovative strengthening techniques and anchorage systems using different materials on flexure performance of R.C beams. *Case Studies in Construction Materials*. https://doi.org/10.1016/j.cscm.2022.e01733
Muciaccia, G., Khorasani, M., & Mostofinejad, D. (2022). Effect of different parameters on the performance of FRP anchors in combination with EBR-FRP strengthening systems: A review. *Construction and Building Materials, 354*, 129181. https://doi.org/10.1016/j.conbuildmat.2022.129181
Ngidi, S. D., & Dundu, M. (2018). Composite action of pre-cracked reinforced concrete beams repaired with adhesive bonded steel plates. *Structures, 14*, 400–408.
Rageh, B. O., El-Mandouh, M. A., Elmasry, A. H., & Attia, M. M. (2022). Flexural behavior of RC beams strengthened with GFRP laminate and retrofitting with novelty of adhesive material. *Buildings*. https://doi.org/10.3390/buildings12091444
Shaheen, Y. B., & Abusafa, H. M. (2017). Structural behavior for rehabilitation ferrocement plates previously damaged by impact loads. *Case Studies in Construction Materials, 6*, 72–90.
Sharaky, I. A., Torres, L., Comas, J., & Barris, C. (2014). Flexural response of reinforced concrete (RC) beams strengthened with near surface mounted (NSM) fiber reinforced polymer (FRP) bars. *Composite Structures, 109*, 8–22.
Shehab, H. K., Eisa, A. S., & El-Awady, K. A. (2017). strengthening of cutouts in existing one-way spanning R. C. flat slabs using CFRP sheets. *International Journal of Concrete Structures and Materials*. https://doi.org/10.1007/s40069-017-0186-7
Smith, S. T., Hu, S., Kim, S. J., & Seracino, R. (2011). FRP-strengthened RC slabs anchored with FRP anchors. *Engineering Structures, 33*(4), 1075–1087.
Tank, T., & Modhera, C. D. (2017). Finite element modelling of RC slab strengthened with GFRP. *Materials Today: Proceedings, 4*(9), 9784–9791.
Thanoon, W. A., Jaafar, M. S., Kadir, M. R. A., & Noorzaei, J. (2005). Repair and structural performance of initially cracked reinforced concrete slabs. *Construction and Building Materials, 19*(8), 595–660.
Wang, J.W. and K.H. Tan. (2002) Punching shear behaviour of RC flats slabs externally strengthened with FRP systems. In: Proceedings of the 5th International Symposium on Fiber Reinforced Plastics for Reinforced Concrete Structures (FRPRCS-5) Vol. 2, Cambridge University, Cambridge, UK. pp: 997–1005, (2002).
Yang, J. Q., Smith, S. T., Wang, Z., & Lim, Y. Y. (2018). Numerical simulation of FRP-strengthened RC slabs anchored with FRP anchors. *Construction and Building Materials, 172*, 735–750.
Zheng, X., Wan, B., Huang, P., & Huang, J. (2019). Experimental study of hybrid strengthening technique using carbon fiber laminates and steel plates for reinforced concrete slabs. *Construction and Building Materials*. https://doi.org/10.1016/j.conbuildmat.2019.03.100
Zhou, Y., Chen, X., Wang, X., Sui, L., Huang, X., Guo, M., & Hu, B. (2020). Seismic performance of large rupture strain FRP retrofitted RC columns with corroded steel reinforcement. *Engineering Structures*. https://doi.org/10.1016/j.engstruct.2020.110744
Zhou, Y., Gao, H., Hu, Z., Qiu, Y., Guo, M., Huang, X., & Hu, B. (2021a). Ductile, durable, and reliable alternative to FRP bars for reinforcing seawater sea-sand recycled concrete beams: steel/FRP composite bars. *Construction and Building Materials, 269*, 121264.
Zhou, Y., Sui, L., Huang, X., Guo, M., Luo, M., Hu, B., et al. (2021b). Enhancing the EB-FRP strengthening effectiveness by incorporating a cracking-control layer of ECC with different thicknesses. *Construction and Building Materials, 286*, 122975. https://doi.org/10.1016/j.conbuildmat.2021.122975

Publisher's Note

Mohamed H. Makhlouf is an Associate Professor, Civil Engineering Department, Benha Faculty of Engineering, Benha University, Egypt.

Ibrahim A. El-Azab is an Assistant Professor, Civil Engineering Department, Benha Faculty of Engineering, Benha University, Egypt.

M. H. Mansour is an Assistant Professor, Civil Engineering Department, Benha Faculty of Engineering, Benha University, Egypt.